

The indication of Martian gully formation processes by slope–area analysis

Susan Conway, Matthew Balme, John Murray, Martin C Towner, Chris H Okubo, Peter M Grindrod

▶ **To cite this version:**

Susan Conway, Matthew Balme, John Murray, Martin C Towner, Chris H Okubo, et al.. The indication of Martian gully formation processes by slope–area analysis. The Geological Society, London, Special Publications, 2011, 356 (1), pp.171-201. 10.1144/SP356.10 . insu-02276823

HAL Id: insu-02276823
https://insu.hal.science/insu-02276823

Submitted on 3 Sep 2019

HAL is a multi-disciplinary open access archive for the deposit and dissemination of scientific research documents, whether they are published or not. The documents may come from teaching and research institutions in France or abroad, or from public or private research centers.

L'archive ouverte pluridisciplinaire **HAL**, est destinée au dépôt et à la diffusion de documents scientifiques de niveau recherche, publiés ou non, émanant des établissements d'enseignement et de recherche français ou étrangers, des laboratoires publics ou privés.

The indication of martian gully formation processes by slope-area analysis.

*Susan J. Conway

Work done at: Earth and Environmental Sciences, Open University, Walton Hall, Milton Keynes MK7 6AA UK tel:+44 (0)1908 659777 fax:+44 (0)1908 655151

Now at: Laboratoire de planétologie et géodynamique, CNRS UMR 6112, Université de Nantes, 2 rue de la Houssinière, BP 92208, 44322 Nantes cedex, France tel : +33 (0)251 125570 Susan.Conway@univ-nantes.fr

Matthew R. Balme

Earth and Environmental Sciences, Open University, Walton Hall, Milton Keynes MK7 6AA UK tel:+44 (0)1908 659776 fax:+44 (0)1908 655151 m.r.balme@open.ac.uk

John B. Murray

Earth and Environmental Sciences, Open University, Walton Hall, Milton Keynes MK7 6AA UK tel:+44 (0)1908 659776 fax:+44 (0)1908 655151 j.b.murray@open.ac.uk

Martin C. Towner

Impacts and Astromaterials Research Centre, Department of Earth Science and Engineering, Imperial College London, SW7 2AZ, UK. tel:+44 (0)20759 47326 fax:+44 (0) 20 7594 7444 m.towner@imperial.ac.uk

Chris H. Okubo

Astrogeology Science Center, U.S. Geological Survey 2255 N. Gemini Dr. Flagstaff, AZ 86001, USA tel:+1 (928) 556-7015 fax:+1 (928) 556-7014 cokubo@usgs.gov

Peter M. Grindrod

Department of Earth Sciences, University College London, Gower Street, London WC1E 6BT UK tel:+44 (0)20 7679 7986 p.grindrod@ucl.ac.uk

*Corresponding author (e-mail: s.j.conway@open.ac.uk)

Number of words: 12 624

Number of References: 180

Number of Tables: 2

Number of Figures: 11

The styles for each heading level:

Heading 1

Heading 2

Heading 3

Running title: Martian gully formation processes.

Abstract

The formation process of recent gullies on Mars is currently under debate. This study aims to discriminate between the proposed formation processes: pure water flow, debris flow and dry mass wasting, through the application of geomorphological indices commonly used in terrestrial geomorphology. We used high resolution digital elevation models of Earth and Mars to evaluate the drainage characteristics of small slope sections. We have used the data from Earth to validate the hillslope, debris flow and alluvial process domains previously found for large fluvial catchments on Earth, and have applied these domains to gullied and ungullied slopes on Mars. In accordance with other studies our results indicate that debris flow is one of the main processes forming the martian gullies that we studied. The source of the water is predominantly distributed surface melting, not an underground aquifer. We also present evidence that other processes may have shaped martian crater slopes, such as ice assisted creep and solifluction, in agreement with proposed recent martian glacial and periglacial climate. Our results suggest that, within impact craters, different processes are acting on differently oriented slopes, but further work is needed to investigate the potential link between these observations and changes in martian climate.

Martian “gully” landforms were first described by Malin & Edgett (2000) and defined as features that have an alcove, channel and debris apron with the general appearance of gullies carved by water. Within this definition gullies have a wide range of morphologies (Fig. 1) and they are found in abundance on steep slopes at mid latitudes in both hemispheres on Mars (e.g., Heldmann & Mellon 2004; Heldmann *et al.* 2007). They are interpreted to be geologically young features because of the pristine appearance and paucity of superposed impact craters. Recent work has suggested that some gullies have been active in the last 3 - 1.25 Ma (Reiss *et al.* 2004; Schon *et al.* 2009). Malin *et al.* (2006) observed new, high-albedo, dendritic deposits (named light-toned deposits) located along the paths of some gullies, and which formed between subsequent images taken by the Mars Orbiter Camera (MOC). These light-toned deposits have been attributed to either dry mass wasting (Pelletier *et al.* 2008; Kolb *et al.* 2010), or debris flow (Heldmann *et al.* 2010), involving up to 50 % water (Iverson 1997). However, the origins of these deposits are still under debate and it is not clear whether they are related to the formation processes of the gullies, or whether they are formed by a secondary process.

The formation process for martian gullies in general is also still under debate. Three main candidates exist: (1) aquifer outflow, (2) surface melting, or (3) dry granular flow. In the aquifer model the water is either released from a near surface confined aquifer (Malin & Edgett 2000; Heldmann *et al.* 2005) or brought up from depth by cryovolcanic processes (Gaidos 2001). The main criticism of the aquifer based models is their failure to explain the location of some gullies on isolated hills, impact crater central peaks, mesas and sand dunes. Melting of near surface ground ice or surface ice has been proposed for the formation of gullies under recent obliquity excursions (Costard *et al.* 2002). There is growing support for this model with the most compelling arguments being: (1) the majority of gullies exists at mid-latitudes, (2) the dominance of pole-facing gullies (Balme *et al.* 2006; Dickson *et al.*

2007; Kneissl *et al.* 2009) and, (3) observations of coincidence with sites of seasonal surface ice accumulation (Dickson & Head 2009). Granular flow has been suggested as either unassisted (Treiman 2003; Shinbrot *et al.* 2004), or carbon dioxide assisted flow (Musselwhite *et al.* 2001). The main criticism of the granular flow model is that it fails to replicate some commonly observed features of gullies, in particular channel sinuosity and complex tributary and distributary systems (McEwen *et al.* 2007).

There is also debate about the type of fluid involved: pure water, or brine. Whilst pure water is not stable under the current surface environment on Mars, it can persist in a metastable form (Hecht 2002), although its flow behaviour may be substantially different to water on Earth (Conway *et al.* 2010a). Brines are a likely product of water sourced from underground and, moreover, the presence of some common geological compounds can substantially depress the freezing point of water (e.g., Chevrier & Altheide 2008). Brines are less likely in a surface melting scenario, because water ice condensed from the atmosphere will have had less opportunity to dissolve salts than an underground water body. Both pure water and brine can support very high concentrations of entrained sediment, and form a flow commonly termed a “debris flow”. Debris flow is an attractive candidate process for forming gullies, because large amounts of erosion and deposition can be brought about with only 10 to 50 % water content (Iverson 1997). Several authors have proposed debris flow as a potential gully-forming mechanism on Mars due to the supply of loose sediment combined with the steep slopes on which gullies are found (e.g., Malin & Edgett 2000; Balme *et al.* 2006). The inclusion of debris might also limit evaporation and freezing of the water within the flow. Debris flows on Earth are commonly triggered by sudden and intense or prolonged rainfall, (e.g., Ben David-Novak *et al.* 2004; Decaulne & Sæmundsson 2007; Godt & Coe 2007; Crosta & Frattini 2008; Morton *et al.* 2008) which is not a possible mechanism on Mars under recent climate. However, debris flows can also be triggered by snowmelt, or melting

permafrost (Harris & Gustafson 1993; Decaulne *et al.* 2005). As noted by Lanza *et al.* (2010) infiltration rates on Mars are likely to exceed the low discharge rates produced by a surface melting source. Hence, overland flow is unlikely, unless there is a shallow impermeable barrier, such as near-surface permafrost, or frozen layer formed at the base of the water flow on contact with a cold substrate (Conway *et al.* 2010a). The dominance of infiltration satisfies the conditions for debris flow triggering, sediment saturation and elevated pore pressures. The lack of vegetation and the associated lower cohesion of the martian soil, compared to Earth, potentially means that debris flows can be triggered on much lower slope gradients than they are on Earth.

Gullies formed by dilute-water flow and debris flow on Earth can be visually very similar to each other, and the basic structure of gullies can be formed by dry granular flow (Mangeney *et al.* 2007). In many geomorphological problems, convergence of visual form means that using images alone can make it very difficult to determine process. The ongoing debate regarding the formation mechanisms of gullies on Mars is a prime example of this. For example some workers have dismissed debris flow as a mechanism for forming martian gullies, because they have not observed the levées that are one of the diagnostic features of debris flow (e.g., Innes 1983). However, the ability to identify levées depends on viewing geometry and sun angle; metre sized levées are often not visible on 25 cm/pixel air photos of Earth. It is also possible that a combination of the lower gravity and different sediment type on Mars means that the levées might be small compared to those on Earth.

The amount of water required to carve channels and transport and deposit sediment differs substantially between debris flow, water or brine flow (termed “alluvial” throughout the rest of this paper) and granular flow. Determining the amount of water available at the martian surface is important for questions of martian climate, hydrology and the study of potential martian habitats. Hence, an accurate determination of active processes is needed that

in turn can constrain the quantity of fluid required to form gullies. Quantitative geomorphological study can provide the tools to discriminate between these three processes. The recent availability of high resolution digital elevation models (DEMs) of Mars has opened up the possibility of using quantitative geomorphic methods that have, until now, been restricted to analysing landscapes on Earth. By taking well-developed slope-area analyses and other geomorphic process indicators for the Earth and applying them to Mars, this study aims to give insights into both the processes that formed the gullies on Mars and the source of any water involved.

We used three geomorphic tools commonly applied in terrestrial geomorphology to identify active processes forming gullies on Mars: slope-area plots (Fig. 2a), Cumulative Area Distribution (CAD) plots (Fig. 2b) and wetness index maps. These analytical techniques are described in more detail in the following sections. They are usually used to assess active processes within catchment areas and other larger-scale landscape analyses. To test whether they are equally applicable to smaller areas, we first applied them to five study sites on Earth at an equivalent scale to gullies on Mars. Recently deglaciated areas were preferred as these have: (1) a geologically short and well defined slope development history (i.e. since deglaciation) and, (2) a glacial trough valley slope-profile which strongly resembles that of fresh impact craters (compare relationships in Brook *et al*. (2008) and Garvin *et al.* (1999). However, suitable quality data could not be found for the alluvial end-member process in glacial environments, so two desert study sites were also included.

When we were satisfied that different geomorphic processes could be discriminated on Earth using slope-area plots, CAD plots and wetness index maps, we applied these analyses to slopes containing gullies on Mars.

Method

Slope-area and Cumulative Area Distribution (CAD) methods

The so-called "stream power law" was first proposed by Hack (1957) and has been widely used to investigate landscape evolution on Earth (e.g., Kirkby *et al.* 2003; Stock & Dietrich 2003). It is based on the detachment and transport limited rate of bedrock erosion, otherwise known as the shear-stress incision model, which is stated as follows:

$$S = kA^{-\theta} \quad (1)$$

where S is local slope, A is upslope drainage area, k is a process related constant, which is different for detachment and transport cases, and θ is the concavity index, which is process dependent. It has also been noted that if the drainage area is plotted against the local slope for drainage basins then process domains can be defined in log-log plots as shown in Fig. 2a (after Montgomery & Foufoula-Georgiou 1993). These process domains were initially schematic, based on few data, but have been supported by later work (e.g., Whipple & Tucker 1999; Snyder *et al.* 2000; Kobor & Roering 2004; Marchi *et al.* 2008). Brardinoni & Hassan (2006) added an additional domain in which systems dominated by debris flow deposition, occupy that part of the alluvial domain of Montgomery & Foufoula-Georgiou (1993), which is located towards higher drainage areas and steeper slopes (Fig. 2a). This domain was proposed from field observations in glacially modified area and has since been supported by additional observations by Mao *et al.* (2009) in a different geomorphic setting. Process information can be obtained both from the position of the data points relative to defined domains on this slope-area plot, and from the trend of the data within these domains, for example, whether the data points plot in a concave, convex, upward trending, or downward trending curve (Tucker & Bras 1998). The general trend for an alluvial system is shown in Fig. 2a, which passes through several process domains. The data for such plots are generally

184 derived from digital elevation models or topographic maps. The slope and contributing area
185 data are either extracted from the channel only, or the whole drainage basin, depending on the
186 focus of the study. In Fig. 2a these data are taken from every pixel contained within the
187 catchment of the whole fluvial system (encompassing valley hillslopes, tributaries, main
188 channels and estuary system) sampled at a single point in time.

189 Cumulative Area Distribution (CAD) is the probability distribution of points in the
190 landscape having a drainage area greater than any particular area, A^*. The log-log plot of
191 $P(A>A^*)$ against A^* gives information on the processes acting within a catchment (Perera &
192 Willgoose 1998; McNamara *et al.* 2006). Interpretation of this index varies, but generally it is
193 split into three areas: (1) at small drainage areas the plot usually evolves from convex to
194 concave, and represents diffusive erosion, (2) intermediate drainage areas are linear in a log-
195 log plot and this is thought to represent incision, (i.e. channel formation), and (3) at large
196 drainage areas there are small steps where major tributaries join the channel (Fig. 2b).
197 McNamara *et al.* (2006) split domain (1) into three sub-domains (Fig.2b): (1a) a convex
198 section, representing hillslopes that diverge and do not gather drainage, (1b) linear and steep
199 section in a log-log plot, indicating hillslopes with convergent topography and, (1c) a
200 concave section, which they suggest is a reach dominated by pore pressure triggered
201 landsliding (including debris flows which are triggered by this mechanism).

202 The stream-power law (Eq. 1), and process interpretations in slope-area and CAD
203 plots of Montgomery & Foufoula-Georgiou (1993), Brardinoni & Hassan (2006) and Tucker
204 & Bras (1998) are based on empirical hydraulic geometry functions that are predicated on,
205 and developed for, studies of large fluvial systems with channel morphology well-adjusted to
206 perennial discharge. It could therefore be argued that these systems are unlike the hillslope
207 systems in this study. Hence, we have tested these interpretive analysis techniques on small
208 gully-systems on Earth where we know the active processes in order to demonstrate that they

209 can still be valid. It is, of course, necessary to bear in mind that there is always some
210 uncertainty in inferring process from landscape form, in part due to the intrinsic variability
211 and complexity of natural systems but also due to the effects of vegetation, tectonics, climate
212 and perhaps human interaction with the landscape. However, on Mars the surface processes
213 are likely to be simpler, with little chance of factors, such as rain, vegetation or human action
214 confounding the process domains, so these indices should provide an important addition to
215 the "visual" morphology when inferring process from form.

216 ## *Application of slope-area method to Mars*

217 The reduced gravitational acceleration of Mars shifts the slope-area boundary of the alluvial
218 slope-area domain vertically (dotted line in Fig. 2a). This means that the unchanneled domain
219 extends to higher slopes for a given drainage area for Mars (extending into the alluvial and
220 debris flow domains for Earth); however the hillslope domain is unaffected. Considering the
221 fact that gullies on Mars do not have large tributary-channel networks it seems unlikely that
222 this domain would be well developed. Appendix 1 gives details of the calculations performed
223 to account for the gravitational acceleration of Mars. The relative gradients and curvatures of
224 the trends described by the alluvial data in slope-area plots are unaffected by the reduced
225 gravity. We have not been able to revise the position of the domain added by Brardinoni &
226 Hassan (2006) as a function of gravitational acceleration because this domain was added
227 empirically, based on field observations.

228 The slope threshold for dry mass wasting or landsliding in loose material is the same
229 as on Earth (Moore & Jakosky 1989; Peters *et al.* 2008). The slope thresholds for pore
230 pressure failure are also unaffected by the difference in gravitational acceleration. Hence
231 there would be no change to these process domains or trends for either dry mass wasting or
232 pore pressure triggered processes such as debris flow.

We note that on Earth, vegetation cover, soil type and geology can have profound impacts on the slope values in a landscape for a given drainage area (Yetemen *et al.* 2010), but we would expect only variations in soil type and geology to affect the data on Mars. Despite these differences in surface properties, basins with similar processes on Earth show a similar pattern or trend of data, but displaced vertically in slope-area plots (Yetemen *et al.* 2010).

Datasets and generation of digital elevation models

Slope-area analysis is only possible with high quality elevation data, preferably at a resolution better than 10 m per pixel, or 1:25 000 map scale (Montgomery & Foufoula-Georgiou 1993; Tarolli & Fontana 2009). For each of the terrestrial sites 1 m resolution DEMs were derived from airborne laser altimeter (LiDAR) data. These were then resampled to 5 m resolution to match the Mars data, as described below. Table 1 lists the data sources for the study sites on Earth. The DEM for NW Iceland was produced from the raw LiDAR point data collected by the UK's Natural Environment Research Council's Airborne Research and Survey Facility in 2007 using techniques described by Conway *et al.* (2010b) and correcting for between-track shifts using methods developed by Akca (2007a, b).

For Mars we used four 1 m resolution DEMs produced using stereo photogrammetry from 25 cm per pixel High Resolution Science Imaging Experiment (HiRISE) images. The DEMs for sites PC, GC, KC and TS were produced by the authors from publically released HiRISE images using methods described by Kirk *et al.* (2008). Significant metre-scale random noise present in the DEMs of sites GC, KC and TS had a detrimental effect on preliminary slope-area analyses. Hence, all the DEMs were resampled to 5 m per pixel before the reanalysis was performed.

The precision of elevation values in the DEMs used here can be estimated based on viewing geometry and pixel scale. For the DEM of site PC, the attendant image pair PSP_004060_1440 (0.255 m/pixel) and PSP_005550_1440 (0.266 m/pixel) have a 12.6º stereoscopic convergence angle. Assuming 1/5 pixel matching error and using a pixel scale of 0.266 m/pixel from the more oblique image, the vertical precision is estimated to be ~ 0.24 m (cf. Kirk *et al.* 2008). DEMs for sites GC, KC and TS have a similar magnitude of vertical precision. The pixel matching error is influenced by signal-to-noise ratio, scene contrast and differences in illumination between images. Pattern noise can also be introduced by the automatic terrain extraction algorithm, especially in areas of low correlation. Manual editing is necessary to correct spurious topography in areas of poor correlation (e.g., smooth, low contrast slopes and along shadows).

Finally, a synthetic crater was constructed to test whether the results from the Mars study sites in general reflected the process, or instead were a result of the geometry imposed by the impact crater setting (all the Mars study areas were on the inner walls of bowl shaped depressions, but none of the ones on Earth were). A 10 km diameter synthetic crater was created by applying a smooth parabolic radial profile, which was derived by fitting curves through ungullied radial profiles of the craters in sites PC and GC. Metre-scale “pink” (also called “1/f”) noise was added to simulate a natural rough surface (Jack 2000).

Derivation of drainage area and local slope

Representative slope sections were chosen in each DEM (Figs. 3 and 4). For Earth, these were chosen to represent end member and intermediate process domains, including dry mass wasting, debris flow and alluvial processes. On Mars, some areas were chosen that covered the complete slope on which gullies are found, whilst others covered a single gully system, or ungullied slope for comparison. Slope sections always included the drainage divide at the top and extended downslope as far as the visible signs of the distal extent of the gully (or slope)

deposits. Where possible lines delineating drainage basins were followed to define the lateral extent of slope sections, but on poorly incised hillslopes this was not always possible and the lateral extent was defined as a straight line. For site KC, on Mars, we chose different configurations of slope sections to test the sensitivity of our analyses to the exact method used to delineate the slope-sections. Careful delineation of slope sections is necessary for two reasons. Firstly, because the larger the sample area, the more processes are included within it, and the more difficult the results will be to interpret. Secondly, if parts of the slope that are integral to the process to be identified are omitted, then the process signal will not be complete.

The slope and the flow directions of each pixel in each DEM were determined using a "Dinf" algorithm. This algorithm gives flow directions in any direction, rather than only towards one of the eight neighbouring pixels (Tarboton *et al.* 1991). This has been shown to produce better results from slope-area analysis because it gives a more accurate approximation of the real path of flow through the landscape (Borga *et al.* 2004). For each pixel, the accumulation of flow was calculated from the flow directions by summing the number of pixels located upstream, and multiplying by the pixel area. These analyses were performed using the TauDEM extension for ArcGIS, based on the algorithms developed by Tarboton (1997). For each DEM the "wetness index" was also calculated. This is the natural logarithm of the ratio of contributing area to slope. It provides information on the potential connectivity of the landscape drainage and the potential ability of the surrounding landscape to route drainage (Woods & Sivapalan 1997). However, in the case of Earth and particularly in the case of Mars this index should not be interpreted literally as implying that the terrain is "wet". In our study it is used as a visual aid to interpret the spatial variability of the slope-area plot. For example, highly permeable talus slopes on Earth are essentially dry, but they may have moderate to high wetness index. However, we would expect a talus slope on Earth

to show a characteristic spatial pattern of wetness index, indicative of dry mass wasting processes. All the DEMs underwent the same processing steps.

We extracted the drainage area and slope for every pixel within the chosen slope sections. To simplify the representation of these data we calculated the mean slope for 0.05 wide logarithmic bins of drainage area, and then constructed the slope-area and CAD plots. Binning data in this way make the trends in slope-area and CAD plots clearer and is a commonly used display technique (e.g., Snyder *et al.* 2000).

In addition, for one site on Mars (site KC), we visually identified the initiation sites of the gullies on orthorectified HiRISE images. The initiation points for the gullies were defined as the furthest upstream extent defined by a distinct cut, or scarp (Fig. 5a). For each of these locations we extracted the slope and drainage area for the underlying pixel. This analysis was not performed for site PC because edge contamination and noise made it impractical. The analysis was also omitted for site GC because the gullies start at the top of the slope, so would by definition occur at the lowest drainage areas.

Study areas

Earth

All the study sites on Earth are located in the northern hemisphere and most are within the continental USA. Table 1 provides a summary of the sites and Fig. 3 shows the setting of the areas studied.

Site SJ – San Jacinto, California

This site is located in California along a splay of the San Andreas fault, called the San Jacinto fault. This area is a desert with little rainfall (~ 150 mm, annual average recorded by NOAA weather station in nearby Borrego Springs), which has undergone rapid recent uplift caused

by the fault system. The landscape has a well developed ephemeral gully network with large alluvial fans. From the study of the 1 m LiDAR data and aerial images we infer the processes forming these fans to be sheet-flow rather than debris flow, based on the lack of levées and lobate terminal deposits. The vegetation is sparse, consisting of small scrub bushes. The underlying geology of the study area is mainly granite, schist and gneiss with minor outcrops of Quaternary older fan deposits (Moyle 1982). For our analyses we used three study areas that contained small complete gully systems, including sources, channels and debris aprons, but avoided large fan systems and debris aprons from neighbouring systems (Figs. 3a and 3b: study areas SJ1, SJ2 and SJ3). Due to the small size of the fans in area SJ1 it is difficult to entirely rule out debris flow as a potential process in forming these alluvial fans.

Site DV - Death Valley, California

This site is located a few kilometres NE of Ubehebe volcano, in Death Valley, California. This is a desert area that has well developed ephemeral gully networks with large alluvial fans. There is little precipitation in this area although the nearby mountains receive as much as 85 mm of rain per year (Crippen 1979) and rare large storms can do much geomorphic work. Debris flows are found on the fans in the area (e.g., Blair 1999, 2000), but the primary process active in the gullies is alluvial transport (Crippen 1979). We inspected the 1 m LiDAR data for presence of levées and depositional lobes on the fans and found no evidence of these. However, without direct field observations the fact that debris flows do not act on these fans remain an assumption. The bedrock consists of Palaeozoic sedimentary rocks (Workman *et al.* 2002). We chose two study areas (Fig. 3c: study areas DV1 and DV2) with gully systems that were not affected by neighbouring alluvial fans or gully systems so only receive local rainfall levels.

Site KA – St Elias Mountains, Alaska

This site is located east of the abandoned town of Katalla close to the recently deglaciated mountain range of St Elias, near the coast of Alaska and on the border with Yukon, Canada. The area has been unglaciated for approximately the last 10 000 years (Sirkin & Tuthill 1987) and receives very high precipitation, which falls as snow on the upper slopes and rain on the lower. Our study area overlies Tertiary volcanic materials. The slope scarp was generated by the active Ragged Mountain Fault (Miller 1961). The area was neither snow covered nor tree covered at the time of survey and the slopes are composed of steep bedrock cliffs that lead directly into large talus aprons. Debris flow tracks are apparent across this talus slope, especially in study areas KA3 and KA4, and might have occurred in study area KA3 as well (Fig. 3d). Study area KA1 has no evidence of debris flow processes (Fig. 3d).

Site FR – Front Range, Colorado

This site is located in the mountainous eastern side of the continental divide. The area was deglaciated around 14 000 to 12 000 years before present (Godt & Coe 2007) and the landscape is dominated by glacially carved valleys. This area has experienced recent debris flows (Coe *et al.* 2002; Godt & Coe 2007) and has no permanent snowpack. Our study slopes, located above the tree line, are dominated by Precambrian biotitic gneiss and quartz monzonite, scattered Tertiary intrusions, and by various surface deposits, all of which host debris flows (Godt & Coe 2007). The head and sidewalls of the cirques have large rockfall talus deposits and which have also experienced recent debris flows. These slopes have little or no vegetation. Three of our study areas (Figs. 3e and 3f: study areas FR2 to FR4) include debris flows located on talus. By way of contrast, we also examined a partially vegetated slope (study area FR1) that is unchanneled and which we infer to be dominated by creep processes (Fig. 3e).

Site WF – Westfjords, Iceland

The site is located in NW Iceland and is dominated by fjords and glacially carved valleys. The last glacial retreat occurred approximately 10 000 years before present (Norðdalh 1990). The valley walls have many active debris flows (Conway *et al.* 2010b) and on the slopes above Ísafjörður (Fig. 3g: study area WF1) they occur in most years (Decaulne *et al.* 2005). The site has a maritime climate, so has high levels of both snow and rainfall, but does not have permanent ice or snow patches. The site is underlain by Miocene basalts, although the debris flows occur most often in glacial till. From this site we chose a study area above the town of Ísafjörður that has very active debris flows (Fig. 3g: study area WF1), two study areas with less active debris flows and more alluvial processes (Figs. 3g and 3h: study areas WF2 and WF3), and one study area dominated by rockfall and rock slide processes, although there are some debris flow tracks visible in the field (Fig. 3h: study area WF4). All these study areas have patchy vegetation, but no trees.

Mars

All the gullies that we studied on Mars were located on the inner walls of craters in the southern hemisphere (Table 2). Slopes both with and without gullies were analysed for comparison. Sites PC, GC and KC were analysed by Lanza *et al.* (2010), because all the sites showed visual evidence of debris flows.

Site PC – Penticton Crater in Eastern Hellas

This site contains the very recent, light-toned deposits observed by Malin *et al.* (2006) and interpreted by them to be a recent “gully forming” event. These flows were later suggested by Pelletier *et al.* (2008) to be produced by dry granular flow, or possibly also debris flow. This slope does not have any well defined channels. We used two study areas within the ~ 7.5 km diameter crater for our slope-area analyses, shown in Figs. 4a and 4b. Study area PC1 is

401 located over the equator-facing light-toned deposits (Fig. 4a) and study area PC2 on the west-
402 facing crater wall which contains small gullies (Fig. 4b). These gullies appear to be incised
403 into “mantle deposits” (Mustard *et al.* 2001). The mantle is hypothesised to be the remnants
404 of a previously extensive volatile rich deposit (e.g., Mangold 2005). This crater is very
405 asymmetric, with the east and north rims being subdued in terms of elevation (the rim is
406 nearly absent on the east side) whilst the southern rim is abrupt and steep.

407 *Site GC – Gasa Crater in Terra Cimmeria*

408 This ~ 7 km wide crater, shown in Figs. 4c and 4d, has well developed alcoves or
409 indentations into the rim of the crater. Gully channels are most obvious on the west-facing to
410 pole-facing slopes (Figs. 4c and 4d) and the equator-facing slope lacks these well defined
411 alcoves and channels (Fig. 4e). We chose sections on the pole- (study areas GC1 and GC2),
412 west- (study area GC3) and equator-facing (study area GC4) slopes. This crater is located
413 within a larger crater, which also has gullies on its west- to pole-facing slopes. There is no
414 evidence of mantle deposits being present anywhere within this crater.

415 *Site KC – crater inside Kaiser Crater in Noachis Terra*

416 The study crater, ~ 12 km across is located within the larger Kaiser crater, which not only has
417 gullies down its own rim, but also gullies on the dunes within it (Bourke 2005). Gullies in
418 this crater have alcoves at various positions on the slope, which converge to form well
419 defined tributary networks. Lateral levées bound some of the channels (Figs. 5b and 5c). This
420 slope has the subdued appearance often attributed to the presence of volatile rich mantle
421 deposits (Mustard *et al.* 2001). We chose study areas that encompass the drainage area of two
422 gullies (study area KC2), a single gully (study area KC1) and also the slope section as a
423 whole (study area KC3), all of which are shown in Fig. 4f. We chose study area KC4, an area
424 of the slope not affected by gullies, for comparison (Fig. 4f).

Site TS – crater in Terra Sirenum

This ~ 7 km diameter crater is located to the south of Pickering Crater in Terra Sirenum and contains pole-facing gullies. We analysed an equator-facing slope (Fig. 4g: study area TS1) which has no evidence of channels but contains an apparently well developed talus apron. There is no evidence of mantle deposits being present on this slope.

Results

Earth

Initially we chose two study areas with talus and with active creep. The slope-area analysis results for these are shown in Fig. 6a. The study areas with well developed talus (WF4 and KA1) show the following pattern on log-log plots: (1) At small drainage area the curves are initially flat. (2) There is then a linear decrease in slope with increasing drainage area. (3) The curve then becomes horizontal again at higher drainage area with a lower slope value. Talus slopes that have a mixture of processes (e.g., KA2) show a curve that drops off linearly in log-log plots then flattens at higher drainage areas.

The CAD plot (Fig. 7a) provides additional information: the talus dominated study areas have a very smooth convex shape. The gradient of the curve is low until the drainage area is between approximately 0.001 km^2 after which the curve drops sharply and continues to steepen with increasing drainage area.

The soil creep diffusive process study area (FR1 in Fig. 6a) shows a distinctive signature in slope-area plots: (1) The curve is initially horizontal to gently downwards sloping. (2) Between drainage areas of 0.0001 to 0.001 km^2 the slope increases linearly with increasing drainage area. (3) There is then a marked slope turnover at which the curve switches to decreasing slope with increasing drainage area. The soil creep diffusive process study area resembles the talus slopes in CAD plots (FR1, Fig. 7a).

Figs. 6b and 7b show the debris flow study areas that are influenced by talus processes and Figs. 6c and 7c show those that are more influenced by alluvial processes. Generally in slope-area plots debris flow produces a curve that drops off linearly in log-log plots, flattening off before finally dropping away steeply. The difference between the talus study areas (e.g. KA2, Fig. 6a) and the debris flow study areas influenced by talus (Fig. 6b) is subtle in some cases. In a similar way the difference between the debris flow areas influenced by talus processes (Fig. 6b) and those influenced by alluvial processes (Fig. 6c) is also subtle. Without field information it would be difficult to differentiate talus dominated and debris flow dominated slopes reliably in slope-area plots (e.g., compare Figs. 6a, KA2 and 6b). However, in CAD plots it is possible to differentiate between the two process types. The debris flow dominated study areas (Figs. 7b and 7c) show the following pattern: (1) The curve drops away from the horizontal slowly (but faster than the talus slopes) at small drainage areas. (2) The curve then either dips down linearly, or follows a flattened convex path, and (3) at high drainage areas the curve drops away sharply with increasing drainage area.

Study areas modified by ephemeral water flow have distinct signatures in slope-area plots (Fig. 6d) and in CAD plots (Fig. 7d). In slope-area plots they show a shallow linearly decreasing trend at small drainage areas, which gets steeper at higher drainage areas, and drops into the alluvial domain. The CAD plot drops away from the horizontal slowly and then dips down linearly (or even with a concave profile) until the tail of the curve drops sharply off at the highest drainage areas.

Synthetic Crater

The slope-area and CAD plots for the synthetic crater are easily differentiated from the process study areas that we have examined on Earth. In slope-area plots the synthetic crater produces a hump-backed curve (Fig. 8d): at small drainage areas the curve rises steeply, then

levels off and drops at high drainage areas. In appearance the curve is, as expected, nearest to study area FR1, the area dominated by diffusive creep (Fig. 6a). In CAD plots (Fig. 9d) the line follows a smooth convex arc, similar to that shown by talus on Earth, except without a break in gradient.

Mars

The slope-area plots for sites PC and GC (Penticton Crater and Gasa Crater inner slopes) closely resemble each one another (Fig. 8a and b). The resulting curve can be divided into three zones: (1) A short initial increase in slope with increasing drainage area, followed by a slope turnover at very small drainage areas. (2) A linear or slightly concave decreasing slope trend with increasing drainage area that continues for most of the plot. (3) Finally, at the largest drainage areas, there is a steep decrease in slope with increasing drainage area. For study area PC1 there is a distinct and linear decline in slope with drainage area, whereas for study areas PC2, GC1, GC2 and GC3 this section is slightly concave. The drop-off at the highest drainage areas occurs at lower absolute drainage area values than for site GC. In the CAD plot, study areas PC1 and GC4 have a smooth convex form, whereas study areas PC2, GC1 and GC2 all have a nearly linear, flattened section at intermediate drainage areas (Figs. 9a and 9b). Study area GC3 lies close to PC1, GC1 and GC2 but without any sign of flattening.

The slope-area plots for gullies in study areas KC1, KC2 and KC3 (Fig. 8c) can be split into three sections as follows: (1) at small drainage areas the curve is sub-horizontal with a subtle upward trend. This trend is more apparent for the data from individual gullies than the data obtained from the whole slope section and is somewhat variable between gully systems. (2) At intermediate drainage areas there is a transitional zone, occurring at different drainage areas for each gully system, in which slope drops off markedly with drainage area.

(3) At higher drainage areas there is a gently declining relationship between slope and drainage area, which is the same for all the gully systems.

The ungullied study area (KC4) is also shown in Fig. 8c. This study area has a hump-back shape, resembling that seen for the synthetic crater. The hump occurs across the same slope values as the transition zone (2) for the gullied slopes. In CAD plots (Fig. 9c) study areas KC2 and KC3 have a flattened section at intermediate drainage areas, followed by a steepening decrease at higher drainage areas. The study area without gullies (KC4) has a curve that is convex and initially declines slowly, before dropping off steeply. Study area KC1 has a less flattened profile than study areas KC2, or KC3 and it seems to be a mixture between slope types typified by gullied study areas KC2 or KC3 and ungullied study area KC4.

In slope-area plots, study area TS1, an ungullied slope, shows a slope-area turnover at small drainage areas, followed by a decreasing and slightly concave trend in slope with drainage area (Fig. 8d). There is a slight upturn at the highest drainage areas, but this is likely to be an artefact caused by few data-points being used to calculate the mean slope in these bins. In CAD plots (Fig. 9d) study area TS1 has a very smooth convex curve.

The slope and drainage area of the gully head initiation points were recorded for site KC. These data are displayed on Fig. 8c. Interestingly, the locations of the gully heads cluster around the range of drainage areas of the transitional section in the slope-area plot, but are located at higher slope values.

Wetness Index on Earth and Mars

The spatial distribution of the slope-area data is most easily visualised using a wetness index map. Maps of wetness index are presented for Earth (Fig. 10) and for Mars (Fig. 11). The alluvial study areas in Earth sites SJ and DV show very low overall wetness indices – only the channels have significant wetness index (Figs. 10a, 10b, and 10c). Debris flow study

areas are slightly more complex (Figs. 10d, 10e, 9f, 10g, and 10h): the slopes generally have moderate wetness index, but there are localised paths along which the wetness index is higher. Site WF (Figs. 10g and 10h) is the best example of this pattern, but it is also the area with the highest influence of overland flow. For site KA (Fig. 10d) this signature is poorly developed, but this site has been influenced by talus processes. The creep dominated study area, FR1, has moderate wetness index throughout (Fig. 10e). The talus study areas KA1, KA2 (Fig. 10d) and WF4 (Fig. 10h) show lobe-like areas of low wetness index with widening streaks of higher wetness index in between.

On Mars, study area PC1 (Fig. 11a) and the synthetic crater (Fig. 11h) have similar wetness index maps: the slope generally increases in wetness index going downhill and there are quasi-linear streaks of higher wetness index that increase in value going downslope. Study area PC2 (Fig. 11b) has overall low wetness index, apart from concentrated lines of high wetness index within the gully alcoves, that spread and become more diffuse in the debris aprons. A similar overall pattern is shown for study areas GC1, GC2 and GC3 (Figs. 11c and 11d), but the ridges around the alcoves have very low wetness index. Study area GC2 in particular (Fig. 11c) shows very concentrated slightly sinuous high wetness index lines on its debris apron. However this part of the DEM contains significant noise, making it hard to judge whether this is simply an artefact. Study areas GC4 (Fig. 11e) and TS1 (Fig. 11g) have similar wetness index maps: there is low wetness index at the crest of the slope and where bedrock is exposed and the wetness index generally increases downslope, but this trend is superposed with diffuse linear streaks of higher relative wetness index. Site KC (Fig. 11f) has generally moderate wetness index, with the alcoves and channels of the gullies showing focussed high wetness index flanked by much lower wetness index and the debris aprons having generally high wetness index with diffuse downslope streaking.

Discussion

Comparison of Earth data to previously published slope-area process domains

There are two interlinked methods of determining slope processes from slope-area plots:
(1) The data points fall within domains in the plots which have been found both theoretically and empirically to relate to particular processes, and
(2) The data points exhibit trends and gradients that provide information on active processes.

We compared our data from Earth to the slope-area process domains of Montgomery & Foufoula-Georgiou (1993) and the additional domain added by Brardinoni & Hassan (2006), shown as solid lines in Fig. 6. The data from our creep, talus and debris flow analyses fall into the debris flow domain of Montgomery & Foufoula-Georgiou (1993). However, some of our debris flow data drop into the alluvial domain at the highest drainage areas. Because they are small systems with limited drainage areas, however, only a few points fall within the alluvial domain. Some of our data approach the additional domain added by Brardinoni & Hassan (2006), but do not extend towards sufficiently high drainage areas (or low drainage areas) to enter it (Fig. 6b and 6c). Our data from the alluvial systems (Fig. 6d) fall into both the debris flow and alluvial domains. They start to trend downwards in slope-area plots at lower drainage areas than our debris flow systems.

Tucker & Bras (1998) simulated the effects of different dominant processes on slope-area plots and we now compare their model results to the patterns in slope-area plots shown by our data. Our talus systems (Fig. 6a) closely fit their model of a landscape dominated by landsliding (which includes the process of debris flow). In slope-area plots our talus data have an initial flat section at small drainage areas, which represents the slope threshold for the rock wall failure and so differs between localities. At higher drainage areas

571 the curves are again flat, representing the failure threshold of loose talus, which is consistent
572 for all areas at approximately 0.7 gradient, equivalent to a slope of approximately 35°. This is
573 an approximate mean slope angle for talus slopes on Earth (Chandler 1973; Selby 1993) and
574 is shown by a dotted horizontal line in Figs. 6 and 8. Between these two horizontal sections
575 there is a transition where the dominance shifts from rock wall failure to unconsolidated talus
576 failure.

577 Within the framework of Tucker & Bras (1998) the pattern shown by the debris flow
578 slopes on Earth (Figs. 6b and 6c) is most consistent with the transition from unsaturated
579 landsliding (dry mass wasting of both talus and rock wall) to pore pressure triggered
580 landsliding (which we interpret to also include debris flow), in a landscape dominated by
581 landsliding. The presence of processes with a slope failure threshold cause data in slope-area
582 plots to fall along horizontal lines. Hence, as the process dominance changes from rock wall
583 failure (highest threshold) to unsaturated landsliding (intermediate threshold) to saturated
584 landsliding (lowest threshold) the curve declines and levels off at the slope value of the
585 saturated landslide threshold in that particular area. As each physical locality has its own
586 saturation threshold this horizontal section occurs at different slope values for different
587 localities but is always located below the dry stability line at 0.7.

588 In slope-area plots, our data from alluvial systems on Earth (Fig. 6d) show a simple
589 decline of slope with drainage area, possibly steepening at higher drainage areas. The data are
590 scattered at drainage areas > 0.001 km^2, due to the limitations of the small sizes of the gully
591 systems available. This means a relatively small number of pixels were used to generate each
592 point, leading to random scatter. However, even taking into account the scatter, the data are
593 below the slope threshold for dry slope failure at 0.7 gradient, which suggests a gradual
594 transition from pore pressure dominated landsliding to fluvial processes.

595 The main feature of our creep dominated hillslope data (FR1, Fig. 6a), is a turnover
596 from increasing slope with drainage area to decreasing slope with drainage area. One of the
597 alluvial systems in site SJ (study area SJ3) shows a weak slope turnover at the lowest
598 drainage areas but none of the other plots show this feature. The slope-area turnover is shown
599 in Fig. 2 and is generally expected to occur in slope-area plots (e.g., Tucker & Bras 1998). It
600 usually occurs in, or close to, the "hillslope" domain of Montgomery & Foufoula-Georgiou
601 (1993). The turnover represents a transition from convex slopes dominated by diffusive
602 processes (which include soil creep often modified by plant roots and other biota) to concave
603 slopes dominated by advective, or alluvial processes. Within the diffusive processes domain
604 in slope-area plots, slope increases with drainage area. The most likely reason that most of
605 our data do not show this turnover is that the slopes we studied lack stable vegetation
606 (Dietrich & Perron 2006; Marchi *et al.* 2008). Another potential contributing factor is that the
607 bedrock and colluvium in our study areas are not naturally cohesive, for example, clay-rich
608 rocks can exhibit convex creep-dominated slopes in unvegetated badlands on Earth.
609 The pattern of data in slope-area plots shown by our alluvial systems and some of
610 our debris flow systems (slow decline at small drainage areas followed by a steep decline at
611 higher drainage areas) has been shown from numerous remote sensing and field studies to
612 mark the transition from the colluvial (including debris flow) regime, to that of a fully fluvial
613 regime (e.g., Lague & Davy 2003; Stock & Dietrich 2003; Stock & Dietrich 2006). Some
614 have described the transition as a separate linear portion of the plot between the colluvial and
615 the fluvial (Lague & Davy 2003) and some as a gradual curved transition (Stock & Dietrich
616 2003). However, both are consistent with Tucker & Bras' (1998) transition from pore
617 pressure triggered landsliding into a fully fluvial system. Our plots do not show a well
618 developed alluvial regime, but this is due to the use of high resolution data of very small
619 areas rather than large, well developed fluvial catchments.

In summary, our terrestrial data are consistent with published slope-area process domains, and provide reassurance that the method is applicable and that the Mars data can be used to infer process in a similar way. The caveat to this is that the environmental differences between Earth and Mars, as detailed in the introduction, must be considered when comparing terrestrial process domains to data from Mars. Furthermore, improved process discrimination can be made by considering CAD profiles in addition to slope-area analysis.

Comparison of Earth data to published CAD process domains

Comparison of all our CAD plots for Earth (Fig. 7) to the published process domains for CAD (Fig. 2) reveals that our data do not generally follow the cited trends. This is possibly because we are studying small areas, rather than large catchments. However, the shape of the curve outlined by our data in CAD plots does allow process discrimination and does follow some of the framework outlined by McNamara *et al.* (2006). Specifically region 1 on Fig. 2 has three sub-regions whose shapes can be recognised in our datasets. The talus data (Fig. 7a) and synthetic crater (Fig. 9d) are both convex in their CAD plots, resembling most closely region 1a of McNamara *et al.* (2006). They describe this region as representing "hillslopes that diverge and do not gather drainage." Our alluvial data and some of our debris flow data show a flattening of the CAD plot curve in the middle region, giving a steep linear section, corresponding to either region 1b or region 2 (Fig. 2b) which McNamara *et al.* (2006) describe as slopes that are convergent (1b), or channel forming (2). Two debris flows (WF2 and WF3 in Fig. 7c) show a concave section, which would correspond to region 1c of McNamara *et al.* (2006) and which they attribute to pore pressure triggered landsliding or debris flow.

The similarity of talus and debris flow in slope-area plots can be attributed to their similarly linear long profiles. However, the two processes produce different patterns in CAD

644 plots because talus slopes tend to disperse drainage but debris flow slopes tend to have
645 convergent drainage. This can also be seen in the wetness index plots (Fig. 10).

646 This difference of behaviour in CAD and wetness index plots, in addition to the
647 information from the slope-area plots, shows that we can detect slopes dominated by alluvial,
648 debris flow and dry mass wasting on the basis of these parameters, even for small catchments
649 such as individual gullies or debris flow tracks. However, it should be noted here that these
650 analyses have been performed on relatively few sample sites on Earth and some of the
651 differences are subtle. Future work has to include extending this analysis to a greater number
652 of test sites on Earth to verify that this kind of process discrimination is robust. Using these
653 initial results we continue and apply these methods of process discrimination to Mars.

654 *Process domains for gullies on Mars*

655 In slope-area plots all the Mars slope sections, except study area TS1, fall below the slope
656 threshold for dry mass wasting (dotted line in the plots in Fig. 8). This means that talus-like
657 dry mass wasting is not a dominant process in these areas. However, study area TS1, visually
658 similar to talus on Earth, is not only above the slope threshold for dry mass wasting, but also
659 bears a signature similar to talus on Earth in the combination of its slope-area plot, CAD plot
660 and wetness index map

661 Within the process domains of Montgomery & Foufoula-Georgiou (1993) the
662 majority of the Mars data lie within the debris flow domain, with some data located in the
663 debris flow deposition domain added by Brardinoni & Hassan (2006) and a few in the
664 alluvial domain. The difference in gravity between Earth and Mars requires an upwards slope
665 adjustment to the alluvial channels domain boundary (see Fig. 2a) in slope-area plots
666 (Appendix 1), but does not change the gradient of the line. This is marked by the dash-dot
667 line on the plots in Fig. 8. This shift places more data in the unchanneled domain, but does
668 not place any additional data into the alluvial or debris flow domains. This in itself

669 distribution does not provide very detailed information on the formation mechanisms for
670 gullies. However, by combining slope-area trends, CAD plots and wetness index maps we
671 can make more detailed assessments. We examine each of the study areas on Mars in turn
672 and then discuss the overall implications for the gully formation processes.

673 *Synthetic Crater*

674 The pattern in slope-area plots of the interior of impact craters is, in part, a result of
675 the inherent shape of the crater slope which in turn is due to the impact process and the
676 modification that occurs immediately afterwards. The slope of a fresh impact crater is
677 concave and exponentially shaped in profile (Garvin *et al.* 1999). Thus in slope-area plots it
678 resembles a well developed alluvial system on Earth (e.g., Hack 1957). This reinforces the
679 uncertainty in inferring a unique process from slope form. In CAD plots, however, the
680 synthetic crater data show a similar pattern to that of talus slopes on Earth, indicating that at
681 short length-scales this type of slope cannot channelise flow on its own. This interpretation is
682 supported by the wetness index plot (Fig. 11), which shows a slowly coalescing flow, rather
683 than discrete areas of fluid concentration.

684 *Site PC – Penticton Crater in Eastern Hellas*

685 In slope-area plots the slope turnover is well expressed for both study areas in site
686 PC (Fig. 8a). This suggests a strong diffusive or creep influence on both slopes. Study areas
687 PC1 and PC2 both resemble either poorly developed talus or debris flow in slope-area plots.
688 In the CAD plot (Fig. 9a); however, study area PC2 has the distinctive profile associated with
689 debris flow, whereas study area PC1 more closely resembles talus. Talus processes can only
690 be active in study area PC1 at small drainage areas, where it lies on the dry mass wasting
691 threshold in slope-area plots. Hence the shape of the CAD curve must be explained by
692 another process, which has a slope threshold but does not concentrate drainage. This

693 unknown process must be pore pressure triggered as it is below the slope for dry mass
694 wasting. In addition, the wetness index plot reveals that study areas PC1 and PC2 are very
695 different: study area PC1 has a similar wetness index map to the synthetic crater (Fig. 11h),
696 whereas study area PC2 resembles debris flow areas on Earth (e.g., Fig. 10f) with strongly
697 concentrated high wetness index within alcoves and channels, becoming more diffuse down
698 slope on the debris aprons.

699 The combined evidence suggests that the west-facing slope, which contains small
700 gullies, has been modified by debris flow, whereas the equator-facing slope is more similar to
701 dry mass wasting deposits. This agrees with the interpretation of Pelletier *et al.* (2008), who,
702 using numerical modelling, concluded that the new bright toned deposits on this slope were
703 more similar in form to deposits of dry granular flows than debris flows.

704 *Site GC – Gasa Crater in Terra Cimmeria*

705 In the slope-area plot for site GC (Fig. 8b), the slope-turnover occurs at very small
706 drainage areas (one or two pixels) and is thus partly abbreviated. This suggests that creep has
707 not strongly influenced this site. This interpretation is supported by the observation that the
708 gully heads originate at the very top of the slope. Study areas GC1, GC2 and GC3 resemble
709 either poorly developed talus on Earth (study area KA2, Fig. 6a) or debris flows on Earth
710 (Figs. 6b and 6c) in slope-area plots. However, in CAD plots (Fig. 9b) they have a flattened
711 mid-section, resembling debris flow systems on Earth. Their wetness index plots (Figs. 11c
712 and 11d) have strong similarities with debris flow systems on Earth (e.g., Fig. 10g): showing
713 flow concentration in the alcove and channel with more diffuse flow on the debris apron.
714 Study area GC2 (Fig. 11c) shows a similar pattern of wetness index to the alluvial systems on
715 Earth, with focussed flow throughout.

716 In slope-area plots (Fig. 8b) study area GC4 has a flatter profile than study areas
717 GC1, GC2 and GC3. The drop in slope at high drainage areas in GC4 is probably an artefact

718 of the low number of pixels included in the slope calculations in the last 5 to 10 points. In the
719 CAD plot (Fig. 9b), study area GC4 has a similar shape to talus systems on Earth (Fig. 7a).
720 The talus interpretation for GC4 is supported by additional evidence: (1) there is no evidence
721 for channels (Fig. 4e), (2) the wetness index plot (Fig. 11e) is similar to talus slopes on Earth
722 and (3) part of the slope-area curve lies on the threshold for dry mass wasting (Fig. 8b). The
723 dip of the slope-area curve away from the threshold for dry mass wasting suggests that
724 another process with a lower slope threshold is acting, either without having an effect on the
725 CAD plot, or with the same CAD plot as talus. We hypothesise that this may be the same
726 unknown process as noted in study area PC1.
727 The combined evidence suggests that the pole and east facing slopes of the crater
728 have been affected by debris flow processes and the equator-facing slope by mass wasting
729 and an unknown process.

730 *Site KC – crater inside Kaiser Crater in Noachis Terra*

731 Our ungullied study area (KC4) shows patterns in slope-area (Fig. 8c) and CAD plots (Fig.
732 9c) very similar to the synthetic crater and creep slopes on Earth. The difference between this
733 study area and the gullied study areas (KC1 to KC3) is presumably a result of the process of
734 gully formation. Study areas KC1 to KC3 do not have slope-area plots (Fig. 8c) that fit easily
735 within the framework established so far. However, if we refer to the modelling work of
736 Tucker & Bras (1998) then the patterns in slope-area plots can be explained. At small
737 drainage areas our curves for study areas with gullies have a horizontal or slightly positive
738 trend compared to our ungullied study area, which has a definite positive trend. This suggests
739 the weak influence of diffusive processes (which generate a positive relationship in slope-
740 area plots) combined with slope threshold processes (which tend to produce horizontal
741 trends). As all the data are below the dry mass wasting threshold, this threshold process is
742 likely to be a pore pressure triggered process, such as debris flow. At intermediate drainage

areas there is a transitional region which occurs at a similar drainage area to the slope-turnover in the ungullied section. At high drainage areas the gullied study areas show a slightly decreasing sub-horizontal trend, as opposed to the ungullied study area which has a well defined decrease in slope with drainage area. This also can be attributed to a pore pressure triggered threshold process but at a lower slope threshold than the previous process. In CAD plots (Fig. 9c) study areas KC1 to KC3 are consistent with debris flow processes. The wetness index plots for these study areas (Fig. 11f) are similar to terrestrial debris flow study areas which have been influenced by alluvial processes (e.g., site WF, Figs. 10g and 10h). This suggests that the first pore pressure threshold in slope-area plots is due to debris flow and the second lower one due to an unknown process, which again could be the same process affecting sites PC and GC.

In slope-area plots, the gully heads on this slope (Fig. 8c) coincide with the drainage area of the slope turnover in study area KC4 and the transitional study areas of KC1 to KC3. This coincident relationship matches the observations made by many authors who have studied gullies on Earth (e.g., Hancock & Evans 2006). Our channel heads lie mainly in the domain attributed to “pore pressure landsliding channel initiation” processes, but some also lie in the “unchanneled” domain (McNamara *et al.* 2006). Notably the gully heads occur below the dry mass wasting threshold, again suggesting that these martian gullies are initiated by a pore pressure threshold process. The gully heads occur on slope gradients of 0.55 similar to those described by Lanza *et al.* (2010), but at drainage areas an order of magnitude lower. This is possibly due to the different approach used by Lanza *et al.* (2010) to measure the contributing area, and possible differences in their interpretation of the location of channel initiation. The co-occurrence of the gully heads with the slope-turnover in slope-area plots suggests that the gullies are a result of whole-slope drainage, as previously found by Lanza *et al.* (2010), either at the surface or shallow subsurface. Our work provides additional evidence

to support the conclusions of Lanza *et al.* (2010) that these gullies originate from a distributed source and hence supports the surface melting model for martian gully formation, rather than an aquifer source model. Further, this observation provides additional evidence that a threshold process, probably debris flow, is forming these gullies, as previously suggested by Lanza *et al.* (2010).

From the combination of the slope-area, CAD and wetness index plots we infer that the gullies in this crater are produced by debris flow and were initiated by surface, or near subsurface, flow of water. Creep and an unknown process were likely to have been the dominant processes on the ungullied crater slopes. This is consistent with the setting of these gullies within the ice-rich mantle deposits which is likely to be susceptible to melting, providing a distributed source of water for the gullies.

Site TS – crater in Terra Sirenum

Unlike the other areas we have studied on Mars, parts of the slope-area data for study area TS1 at lower drainage areas (Fig. 8d) are above the threshold slope for dry mass wasting. This is an indication that rock strength limited dry mass wasting is occurring in the upper parts of the slope. In CAD plots (Fig. 9d) this study area has the classic shape of a talus or creep slope. However, the slope-area trend shown by study area TS1 is very different from that of the synthetic crater (Fig. 8d), which we assume to have been similar to the starting point for study area TS1. This assumption carries the implication that the slope in study area TS1 has evolved over time from concave to linear in profile. Study area TS1 shows a very similar trend in slope-area plots as study area GC4 (Fig. 8b), but originates above the 0.7 slope threshold. As discussed previously for study area GC4, in the framework of Tucker & Bras (1998) such a pattern is likely to reflect a gradual transition from the dominance of a dry mass wasting threshold at lower drainage areas to the dominance of a pore pressure triggered slope threshold due to an unknown process at higher drainage areas. However, in the case of

TS1 this signal not only includes dry mass wasting of non-cohesive material, but rockwall mass wasting as well. The wetness index map shows that the slope does not concentrate drainage, except for some diffuse linear areas, again resembling talus slopes on Earth. The combination of the slope-area plot, CAD plot and wetness index map suggests a dominantly dry mass wasting evolution of this slope, which fits well with the visual observations.

Solifluction on slopes on Mars

In many of the Mars study sites we have inferred an unknown process that is responsible for a second, lower-slope pore pressure triggered threshold in the slope-area plots. However, this process seems to produce slopes that yield a CAD plot that is similar to talus on Earth, i.e. it does not concentrate drainage. As suggested by Tucker & Bras (1998) another threshold process which would produce a similar response in slope-area plots to pore pressure induced landsliding is solifluction. Solifluction in frozen landscapes comprises the combined action of gelifluction and frost creep, and describes the slow, down slope movement of water saturated debris or soils. Solifluction requires freezing and thawing to generate elevated pore pressures and occurs at lower slope angles than pore pressure induced failure, which can trigger landslides and debris flow (Harris *et al.* 2008). This process is consistent with the recent observations of periglacial landform assemblages on Mars (Balme & Gallagher 2009; Balme *et al.* 2009; Soare & Osinski 2009).

Implications for the formation process of martian gullies

Dietrich & Perron (2006) suggested that the lack of biotic processes on Mars would promote erosion by rilling and gullying and stripping of the fine surface materials, given a suitable water source. This would lead to a slope-area plot that lacked a distinct slope turnover, similar to the slope-area plots seen in the Death Valley data (our site DV – Fig. 6d). However, inspecting the trends in the slope-area plots for the Mars systems in Fig. 8, one of

817 the most apparent differences from Earth is the presence of this slope turnover. This indicates
818 that creep is a more dominant process on martian hillslopes than on those we studied on
819 Earth; contradictory to the predictions made by Dietrich & Perron (2006). The creep signal
820 in most published slope-area plots on Earth is induced predominantly by biota, hence on
821 Mars the creep must be facilitated using a different mechanism. Perron *et al.* (2003) observed
822 using Mars Orbiter Laser Altimeter (MOLA) data that slopes on Mars have average gradients
823 well below 35° and suggested that ice driven creep is the cause. Other potential creep
824 mechanisms include frost heave and shrink-swell in clays and hydrated salts, both of which
825 produce creep on un-vegetated and un-bioturbated slopes on Earth. These mechanisms
826 however would require widespread and relatively large amounts of liquid water, which is
827 considered unlikely under current or geologically recent martian climate. Hence, we believe
828 that ice driven creep provides the best explanation for the signals seen in our slope-area data
829 from Mars. In accordance with their results, most of the slopes we studied on Mars also have
830 average gradients well below 35°, with the exception of slope TS1, whose average gradients
831 are partially above 35°.

832 Virtually every gully that we have studied on Mars has the distinct signal of debris
833 flow as the dominant gully forming process. Lanza *et al.* (2010) also found visual and
834 morphometric evidence of debris flows in these areas. The notable exception is area PC1, the
835 slope containing the new light-toned deposits. However, this area does not include gullies of
836 a normal form (Fig. 1) as they lack well defined alcoves and channels. Examination of a far
837 greater number of DEMs containing gullies would be needed to confirm debris flow as the
838 main gully forming process on Mars. However, if this is the principal mechanism, brings up
839 the following hypotheses and predictions for the formation of gullies on Mars:

840 (1) The high sediment concentrations and low infiltration rates could protect the water
841 from evaporation.

842 (2) The energy released by grain interactions within the flow could retard freezing.

843 (3) Basal freezing (Conway *et al.* 2010a) or a permafrost layer could facilitate the
844 saturation of the sediment that is required to generate the high pore water pressures
845 to trigger debris flow.

846 (4) Expected depositional features include levées and lobes.

847 (5) Expected erosional features include discrete slip scars.

848 Points 1-3 of are hard to observe or test, but the erosional and depositional features
849 can be detected in the high resolution HiRISE images. Failure scars have been noted by other
850 authors (Dickson & Head 2009) from HiRISE images and are present within our study areas.
851 Depositional lobes have also been noted by other authors (Levy *et al.* 2009; Lanza *et al.*
852 2010). Visual observations have been made of debris flow levées (Lanza *et al.* 2010), but
853 DEMs from HiRISE are not yet of sufficient quality to reliably resolve debris flow levées.
854 High quality DEMs would allow the estimation of individual flow volumes (Conway *et al.*
855 2010b), which could be used to constrain models of gully formation. This should be a priority
856 for future work, as it would allow more accurate estimates of the amounts of water associated
857 with formation of gully landforms.

858 A debris flow, once triggered, results in more erosion and deposition with less water
859 than pure water flow. This means that high discharges, invoked by other workers (Heldmann
860 *et al.* 2005; Hart *et al.* 2009), are not required to form martian gullies. Modelling has shown
861 that surface melting produces only small amounts of liquid water (Williams *et al.* 2009). This
862 has been one of the major criticisms of the surface melting model. However, if gullies are
863 formed mainly by debris flow, points (1) and (2) above indicate that relatively small amounts
864 of water are needed.

Implications for the water source of martian gullies

The observed relationship in slope-area plots between the slope turnover and the location of gully heads in site KC on Mars is an important observation and indicates that the transition from concave to convex topography is closely linked to gully formation. This would not be expected in an aquifer system, as channel formation would be controlled predominantly by the location of aquifer bodies rather than the shape of the landscape (Fetter 2001). Our work indicates that a widely distributed source of surface or shallow subsurface flow in site KC would be the most satisfactory explanation, in support of the conclusions of Lanza *et al.* (2010). Because our data do not show a definite trend in slope-area plots this indicates that the channels originate from shallow sub-surface flow (Hattanji *et al.* 2006; Jaeger *et al.* 2007; Imaizumi *et al.* 2010), or more likely surface flow in a soil poor landscape (Larsen *et al.* 2006). A potential source for this near surface water is the mantle deposits, which have been observed on both this slope and in site PC2 and has been linked to gully formation by other authors (Christensen 2003; Aston *et al.* 2010; van Gasselt *et al.* 2010).

The development of equally spaced incised alcoves in site GC can either be attributed to geological controls (e.g., faulting), or landscape self organisation from an interlinked debris flow-alluvial system (Perron *et al.* 2009). We argue against a structural control, because there is a lack of these organised alcoves on the equator-facing slope. Hence, considering that we conclude debris flow to be the dominant gully forming process on this crater slope, it would seem most likely that these self-organised alcoves are a result of this process. This kind of self organisation requires a landscape that responds to a distributed water source as on Earth rather than an aquifer source.

Kreslavsky & Head (2003) and Kreslavsky *et al.* (2008) found that pole-facing slopes between 40-50° latitude in both hemispheres were systematically gentler than equator-facing slopes. They suggest that this is due to insolation asymmetry and melting of ice on

pole-facing slopes during periods of high obliquity, similar to the model proposed by Costard *et al.* (2002) for gully formation on pole-facing slopes. Our study sites also show this asymmetry: pole-facing slopes are longer and have a greater variety of slope angles and are more concave, whereas the equator-facing slopes are shorter and have a more uniform distribution of slopes and are more linear. There is a marked difference in geomorphological process between crater walls with different aspects in the two craters that we studied (sites PC and GC). The observed asymmetry of process and form supports the model of a climatic influence on gully formation and general slope development of the craters. However, many more sites would have to be studied to verify this for gullies in general.

Conclusions

We have shown the potential of applying quantitative geomorphological analysis techniques commonly used on Earth for discriminating between different active processes on Mars. Specifically we have validated the use of slope-area plots, cumulative area distribution (CAD) plots, and wetness index maps on small slope sections of less than one square kilometre. We have shown that pure water (alluvial) flow, debris flow and dry mass wasting dominated slopes can be satisfactory discriminated on Earth. By applying these techniques to four areas of Mars containing recent gullies we have inferred that debris flow is the dominant gully forming process. However, we have also inferred that, as on Earth, gully formation on Mars is a complex process: slopes on Mars are likely to have been affected by a variety of processes that lead to a mixture of signals from our geomorphological analyses. Despite this, we have not found the distinctive geomorphological fingerprint of pure water flow on slopes that host gullies. Its absence, however, does not prove the absence of the process. Our results are consistent with the possibility that ice driven creep and solifluction are, or have recently been, active in modifying crater slopes on Mars.

From the location of gully heads within the landscape, and by studying the form of alcoves, it is apparent that at least two of the sites examined contain gullies which have been formed from a widely distributed source of water. This is most easily explained by a surface melting source for the water. The model of Costard *et al.* (2002) provides a mechanism by which the cause of this melting was increased insolation during past high obliquity excursions. Our preliminary observations of an asymmetry in process and form around the impact craters provides additional support for this model, but we cannot rule out surface melting at present day, or during other epochs.

Our geomorphological evidence for debris flow as an active process in forming gullies is reinforced by visual observations. Debris flow as a process leaves distinct geomorphological features, such as failure scars and lobate deposits, which have been observed both here and in previous studies (Dickson & Head 2009; Levy *et al.* 2009; Lanza *et al.* 2010). Unfortunately the topographic data on Mars are not yet sufficient for the discrimination of these features and flanking levées in DEMs, which would allow accurate estimation of individual flow volumes and thus estimation of the volumes of water needed to form the gullies (Conway *et al.* 2010b).

Appendix 1

The derivation of the shear stress erosion model relies on the assumption that erosion rate (E) is a power law of bed shear stress (τ_b):

$$E = k\,\tau_b^{\,a} \qquad (2)$$

where k and a are positive constants. Following Snyder (2000), Whipple & Tucker (1999) we use the assumptions of conservation of mass (water) and steady uniform flow to obtain the following expression of basal shear stress:

$$\tau_b = \rho C_f^{1/3} \left(\frac{gSQ}{W} \right)^{2/3} \quad (3)$$

where ρ is the density of water, C_f is a dimensionless friction factor, g is the acceleration due to gravity, S is the local channel slope, Q is the stream discharge and W is the stream width. We then include a relationship for basin hydrology and hydraulic geometry given by:

$$Q = k_q A^c \quad (4)$$

$$W = k_w Q^b \quad (5)$$

where k_q and k_w are constants, A is the drainage area and b and c are positive dimensionless constants. Combining 2-5, leads to:

$$E = k_e A^m S^n \quad (6)$$

where:

$$k_e = k_b k_w^{-2a/3} k_q^{2a(1-b)/3} \rho^a g^{2a/3} \quad (7)$$

$$m = (2ac/3)(1-b) \quad (8)$$

$$n = 2a/3 \quad (9)$$

Given this, if we now define a constant k_m for Mars, based on the assumption that gravitation acceleration is approximately one third that on Earth:

$$k_m = (1/3)^{2a/3} k_e = (1/3)^n k_e \quad (7)$$

To derive (1), in the main text, we have to include the expectation that over long timescales, uplift rate (U) and erosion rate compete to change the landscape elevation (z):

$$\frac{\partial z}{\partial t} = U - E = U - k_e A^m S^n \quad (8)$$

where t is a given time-step. Now if we assume that the system is in equilibrium in which erosion is balanced by uplift rate, $\partial z / \partial t = 0$, then:

$$S = (U/k_e)^{1/n} A^{-m/n} \quad (9)$$

Comparing this to equation (1), in the main text, we have:

$$k = (U/k_e)^{1/n} \quad (10)$$

$$\theta = -m/n \quad (11)$$

If we then include our k_m constant (7) for Mars in (9) we get:

$$S = (U/k_m)^{1/n} A^{-m/n} \quad (12)$$

$$S = 3(U/k_e)^{1/n} A^{-m/n} \quad (13)$$

Thus for a given drainage area on Earth we would expect the slope on Mars to be three times smaller. Or, in log-log terms:

$$Log\ S = log3 + 1/n\ log(U/ke) - m/n\ logA \quad (14)$$

Acknowledgements

Thanks go to Grant Meyer and one anonymous reviewer for their constructive comments which greatly improved this manuscript. This work would not have been possible without a postgraduate studentship grant from the U.K. Natural Environment Research Council (NERC). We thank the NERC ARSF for obtaining the LiDAR data on which part of this paper relies. We thank the UK NASA RPIF-3D Facility at UCL for enabling the production of one of the HiRISE DEMs. Additional funding was awarded to S.J.C. by Earth and Space Awards, the Geological Society's W.G. Fearnsides Award, The Dudley Stamp Fund and the British Society for Geomorphology's postgraduate funds. P.M.G. is funded by an STFC Aurora Fellowship (ST/F011830/1).Thanks to Jon Yearsley for creation of spatialPattern script to create pink noise in MatLab.

References

Akca, D. 2007a. *Least Squares 3D Surface Matching*. PhD thesis, Eidgenössische Technische Hochschule, Zürich.

Akca, D. 2007b. Matching of 3D surfaces and their intensities. *ISPRS Journal of Photogrammetry and Remote Sensing*, **62**, 2, 112-121.

Aston, A. H., Conway, S. J. & Balme, M. R. 2010. Identifying Martian gully evolution. *In:* Balme, M., Bargery, A. S., Gallagher, C. & Gupta, S. (eds), *Geomorphology on Mars and Other Planets*. The Geological Society of London, accepted.

Balme, M., Mangold, N., Baratoux, D., Costard, F., Gosselin, M., Masson, P., Pinet, P. & Neukum, G. 2006. Orientation and distribution of recent gullies in the southern hemisphere of mars: Observations from High Resolution Stereo Camera/Mars Express (HRSC/MEX) and Mars Orbiter Camera/Mars Global Surveyor (MOC/MGS) data. *Journal of Geophysical Research - Planets;* , **111**, E5, doi:10.1029/2005JE002607

Balme, M. R. & Gallagher, C. 2009. An equatorial periglacial landscape on Mars. *Earth and Planetary Science Letters*, **285**, 1-2, 1-15.

Balme, M. R., Gallagher, C. J., Page, D. P., Murray, J. B. & Muller, J. P. 2009. Sorted stone circles in Elysium Planitia, Mars: Implications for recent martian climate. *Icarus*, **200**, 1, 30-38.

Ben David-Novak, H., Morin, E. & Enzel, Y. 2004. Modern extreme storms and the rainfall thresholds for initiating debris flows on the hyperarid western escarpment of the Dead Sea, Israel. *Geological Society of America Bulletin*, **116**, 5-6, 718-728.

Blair, T. C. 1999. Cause of dominance by sheetflood vs. debris-flow processes on two adjoining alluvial fans, Death Valley, California. *Sedimentology*, **46**, 6, 1015-1028.

Blair, T. C. 2000. Sedimentology and progressive tectonic unconformities of the sheetflood-dominated Hell's Gate alluvial fan, Death Valley, California. *Sedimentary Geology*, **132**, 3-4, 233-262.

Borga, M., Tonelli, F. & Selleroni, J. 2004. A physically based model of the effects of forest roads on slope stability. *Water Resources Research*, **40**, 12, 1-9.

Bourke, M. C. 2005. Alluvial Fans on Dunes in Kaiser Crater Suggest Niveo-Aeolian and Denivation Processes on Mars. *Lunar and Planetary Science Conference*, **36**, no. 2373.

Brardinoni, F. & Hassan, M. A. 2006. Glacial erosion, evolution of river long profiles, and the organization of process domains in mountain drainage basins of coastal British Columbia. *Journal of Geophysical Research - Earth Surface,* **111**, 1, doi:10.1029/2005JF000358.

Brook, M. S., Kirkbride, M. P. & Brock, B. W. 2008. Temporal constraints on glacial valley cross-profile evolution: Two Thumb Range, central Southern Alps, New Zealand. *Geomorphology*, **97**, 1-2, 24-34.

Chandler, R. J. 1973. The Inclination of Talus, Artic Talus terraces, and Other Slopes Composed of Granular Materials. *Journal of Geology*, **81**, 1-14.

Chevrier, V. & Altheide, T. S. 2008. Low temperature aqueous ferric sulfate solutions on the surface of Mars. *Geophysical Research Letters*, **35**, L22101, L22101

Christensen, P. R. 2003. Formation of recent martian gullies through melting of extensive water-rich snow deposits. *Nature*, **422**, 6927, 45-48.

1048 Coe, J. A., Godt, J. W. & Henceroth, A. J. 2002. *Debris Flows along the Interstate 70*
1049 *Corridor, Floyd Hill to the Arapahoe Basin Ski Area, Central Colorado – A Field*
1050 *Trip Guidebook*. U.S. Geological Survey Open-File Report, USGS, Open-File Report
1051 02-398.
1052 Conway, S. J., Balme, M. R., Lamb, M. P., Towner, M. C. & Murray, J. B. 2010a. Enhanced
1053 runout and erosion by overland flow under subfreezing and low pressure conditions:
1054 experiments and application to Mars. *Icarus*, **in review**.
1055 Conway, S. J., Decaulne, A., Balme, M. R., Murray, J. B. & Towner, M. C. 2010b. A new
1056 Approach to Estimating Hazard posed by Debris Flows in the Westfjords of Iceland.
1057 *Geomorphology*, **114**, 4, 556-572.
1058 Costard, F., Forget, F., Mangold, N. & Peulvast, J. P. 2002. Formation of recent Martian
1059 debris flows by melting of near-surface ground ice at high obliquity. *Science*, **295**,
1060 5552, 110-113.
1061 Crippen, J. R. 1979. *Potential hazards from floodflows and debris movement in the Furnace*
1062 *Creek area, Death Valley National Monument, California-Nevada*. U.S. Geological
1063 Survey Open-File Report, **79-991**, USGS.
1064 Crosta, G. B. & Frattini, P. 2008. Rainfall-induced landslides and debris flows. *Hydrological*
1065 *Processes*, **22**, 4, 473-477.
1066 Decaulne, A., Sæmundsson & Pétursson, O. 2005. Debris flow triggered by rapid snowmelt:
1067 A case study in the Gleiðarhjalli area, northwestern Iceland. *Geografiska Annaler.*
1068 *Series A, Physical Geography*, **87A**, 4, 487-500.
1069 Decaulne, A. & Sæmundsson 2007. Spatial and temporal diversity for debris-flow
1070 meteorological control in subarctic oceanic periglacial environments in Iceland. *Earth*
1071 *Surface Processes and Landforms*, **32**, 1971-1983.
1072 Dickson, J. L., Head, J. W. & Kreslavsky, M. 2007. Martian gullies in the southern mid-
1073 latitudes of Mars: Evidence for climate-controlled formation of young fluvial features
1074 based upon local and global topography. *Icarus*, **188**, 315-323.
1075 Dickson, J. L. & Head, J. W. 2009. The formation and evolution of youthful gullies on Mars:
1076 Gullies as the late-stage phase of Mars' most recent ice age. *Icarus*, **204**, 1, 63-86.
1077 Dietrich, W. E. & Perron, J. T. 2006. The search for a topographic signature of life. *Nature*,
1078 **439**, 7075, 411-418.
1079 Fetter, C. W., 2001. *Applied Hydrogeology*. Prentice Hall, New Jersey, 598 pp.
1080 Gaidos, E. J. 2001. Cryovolcanism and the recent flow of liquid water on Mars. *Icarus*, **153**,
1081 1, 218-223.
1082 Garvin, J. B., Sakimoto, S. E. H., Schnetzler, C. & Frawley, J. J. 1999. Global Geometric
1083 Properties of Martian Impact Craters: A Preliminary Assessment Using Mars Orbiter
1084 Laser Altimeter (MOLA). *The Fifth International Conference on Mars, July 19-24,*
1085 *1999, Pasadena, California*, abstract no.6163.
1086 Godt, J. W. & Coe, J. A. 2007. Alpine debris flows triggered by a 28 July 1999 thunderstorm
1087 in the central Front Range, Colorado. *Geomorphology*, **84**, 1-2, 80-97.
1088 Hack, J. T. 1957. Studies of longitudinal stream profiles in Virginia and Maryland. *U.S.*
1089 *Geological Survey Professional Paper*, **294-B**, 45-97.
1090 Hancock, G. R. & Evans, K. G. 2006. Channel head location and characteristics using digital
1091 elevation models. *Earth Surface Processes and Landforms*, **31**, 7, 809-824.
1092 Harris, C., Smith, J. S., Davies, M. C. R. & Rea, B. 2008. An investigation of periglacial
1093 slope stability in relation to soil properties based on physical modelling in the
1094 geotechnical centrifuge. *Geomorphology*, **93**, 3-4, 437-459.
1095 Harris, S. A. & Gustafson, C. A. 1993. Debris flow characteristics in an area of continuous
1096 permafrost, St. Elias Range, Yukon Territory. *Zeitschrift für Geomorphologie,*, **37**, 1,
1097 41-56.

1098 Hart, S. D., Gulick, V. C., Parsons, R. A. & Barnhart, C. J. 2009. Gully Slopes and
1099 Discharges on Lyot Crater's Central Peak. *Lunar and Planetary Science Conference*,
1100 **40**, no. 2349.
1101 Hattanji, T., Onda, Y. & Matsukura, Y. 2006. Thresholds for bed load transport and channel
1102 initiation in a chert area in Ashio Mountains, Japan: An empirical approach from
1103 hydrogeomorphic observations. *Journal of Geophysical Research - Earth Surface*,
1104 **111**, 2, doi:10.1029/2004JF000206.
1105 Hecht, M. H. 2002. Metastability of liquid water on Mars. *Icarus*, **156**, 2, 373-386.
1106 Heldmann, J. L. & Mellon, M. T. 2004. Observations of martian gullies and constraints on
1107 potential formation mechanisms. *Icarus*, **168**, 2, 285-304.
1108 Heldmann, J. L., Toon, O. B., Pollard, W. H., Mellon, M. T., Pitlick, J., McKay, C. P. &
1109 Andersen, D. T. 2005. Formation of Martian gullies by the action of liquid water
1110 flowing under current Martian environmental conditions. *Journal of Geophysical*
1111 *Research - Planets*, **110**, E5, doi:10.1029/2004JE002261.
1112 Heldmann, J. L., Carlsson, E., Johansson, H., Mellon, M. T. & Toon, O. B. 2007.
1113 Observations of martian gullies and constraints on potential formation mechanisms II.
1114 The northern hemisphere. *Icarus*, **188**, 324-344.
1115 Heldmann, J. L., Conley, C., Brown, A. J., Fletcher, L., Bishop, J. L. & McKay, C. P. 2010.
1116 Possible Liquid Water Origin for Atacama Desert Mudflow and Recent Gully
1117 Deposits on Mars. *Icarus*, **206**, 2, 685-690.
1118 Imaizumi, F., Hattanji, T. & Hayakawa, Y. S. 2010. Channel initiation by surface and
1119 subsurface flows in a steep catchment of the Akaishi Mountains, Japan.
1120 *Geomorphology*, **115**, 1-2, 32-42.
1121 Innes, J. L. 1983. Debris Flows. *Progress in Physical Geography*, **7**, 469-501.
1122 Iverson, R. M. 1997. The physics of debris flows. *Reviews of Geophysics*, **35**, 3, 245-296.
1123 Jack, J. L. 2000. Red-shifts and red herrings in geographical ecology. *Ecography*, **23**, 1, 101-
1124 113.
1125 Jaeger, K. L., Montgomery, D. R. & Bolton, S. M. 2007. Channel and perennial flow
1126 initiation in headwater streams: Management implications of variability in source-area
1127 size. *Environmental Management*, **40**, 5, 775-786.
1128 Kirk, R. L., Howington-Kraus, E., Rosiek, M. R., Anderson, J. A., Archinal, B. A., Becker,
1129 K. J., Cook, D. A., Galuszka, D. M., Geissler, P. E., Hare, T. M., Holmberg, I. M.,
1130 Keszthelyi, L. P., Redding, B. L., Delamere, W. A., Gallagher, D., Chapel, J. D.,
1131 Eliason, E. M., King, R. & McEwen, A. S. 2008. Ultrahigh resolution topographic
1132 mapping of Mars with MRO HiRISE stereo images: Meter-scale slopes of candidate
1133 Phoenix landing sites. *Journal of Geophysical Research - Planets*, **113**,
1134 doi:10.1029/2007JE003000.
1135 Kirkby, M. J., Bull, L. J., Poesen, J., Nachtergaele, J. & Vandekerckhove, L. 2003. Observed
1136 and modelled distributions of channel and gully heads - with examples from SE Spain
1137 and Belgium. *Catena*, **50**, 2-4, 415-434.
1138 Kneissl, T., Reiss, D., van Gasselt, S. & Neukum, G. 2009. Distribution and orientation of
1139 northern-hemisphere gullies on Mars from the evaluation of HRSC and MOC-NA
1140 data. *Earth and Planetary Science Letters*, **In Press, Corrected Proof**.
1141 Kobor, J. S. & Roering, J. J. 2004. Systematic variation of bedrock channel gradients in the
1142 central Oregon Coast Range: Implications for rock uplift and shallow landsliding.
1143 *Geomorphology*, **62**, 3-4, 239-256.
1144 Kolb, K. J., Pelletier, J. D. & McEwen, A. S. 2010. Modeling the formation of bright slope
1145 deposits associated with gullies in Hale Crater, Mars: Implications for recent liquid
1146 water. *Icarus*, **205**, 1, 113-137.

Kreslavsky, M. A. & Head, J. W. 2003. North-south topographic slope asymmetry on Mars: Evidence for insolation-related erosion at high obliquity. *Geophysical Research Letters*, **30**, 15, doi:10.1029/2003GL017795.

Kreslavsky, M. A., Head, J. W. & Marchant, D. R. 2008. Periods of active permafrost layer formation during the geological history of Mars: Implications for circum-polar and mid-latitude surface processes. *Planetary and Space Science*, **56**, 2, 289-302.

Lague, D. & Davy, P. 2003. Constraints on the long-term colluvial erosion law by analyzing slope-area relationships at various uplift rates in the Siwaliks Hills (Nepal). *Journal of Geophysical Research - Solid Earth*, **108**, 2, doi:10.1029/2002JB001893.

Lanza, N. L., Meyer, G. A., Okubo, C. H., Newsom, H. E. & Wiens, R. C. 2010. Evidence for debris flow gully formation initiated by shallow subsurface water on Mars. *Icarus*, **205**, 1, 103-112.

Larsen, I. J., Pederson, J. L. & Schmidt, J. C. 2006. Geologic versus wildfire controls on hillslope processes and debris flow initiation in the Green River canyons of Dinosaur National Monument. *Geomorphology*, **81**, 1-2, 114-127.

Levy, J. S., Head, J. W., Dickson, J. L., Fassett, C. I., Morgan, G. A. & Schon, S. C. 2009. Identification of gully debris flow deposits in Protonilus Mensae, Mars: Characterization of a water-bearing, energetic gully-forming process. *Earth and Planetary Science Letters*, **In Press, Corrected Proof**.

Malin, M. C. & Edgett, K. S. 2000. Evidence for recent groundwater seepage and surface runoff on Mars. *Science*, **288**, 5475, 2330-2335.

Malin, M. C., Edgett, K. S., Posiolova, L. V., McColley, S. M. & Dobrea, E. Z. N. 2006. Present-day impact cratering rate and contemporary gully activity on Mars. *Science*, **314**, 5805, 1573-1577.

Mangeney, A., Bouchut, F., Thomas, N., Vilotte, J. P. & Bristeau, M. O. 2007. Numerical modeling of self-channeling granular flows and of their levee-channel deposits. *Journal of Geophysical Research - Earth Surface*, **112**, 2, doi:10.1029/2006JF000469.

Mangold, N. 2005. High latitude patterned grounds on Mars: Classification, distribution and climatic control. *Icarus*, **174**, 336-359.

Mao, L., Cavalli, M., Comiti, F., Marchi, L., Lenzi, M. A. & Arattano, M. 2009. Sediment transfer processes in two Alpine catchments of contrasting morphological settings. *Journal of Hydrology*, **364**, 1-2, 88-98.

Marchi, L., Dalla Fontana, G., Cavalli, M. & Tagliavini, F. 2008. Rocky headwaters in the Dolomites, Italy: Field observations and topographic analysis. *Arctic Antarctic and Alpine Research*, **40**, 4, 685-694.

McEwen, A. S., Hansen, C. J., Delamere, W. A., Eliason, E. M., Herkenhoff, K. E., Keszthelyi, L., Gulick, V. C., Kirk, R. L., Mellon, M. T., Grant, J. A., Thomas, N., Weitz, C. M., Squyres, S. W., Bridges, N. T., Murchie, S. L., Seelos, F., Seelos, K., Okubo, C. H., Milazzo, M. P., Tornabene, L. L., Jaeger, W. L., Byrne, S., Russell, P. S., Griffes, J. L., MartÃ-nez-Alonso, S., Davatzes, A., Chuang, F. C., Thomson, B. J., Fishbaugh, K. E., Dundas, C. M., Kolb, K. J., Banks, M. E. & Wray, J. J. 2007. A closer look at water-related geologic activity on Mars. *Science*, **317**, 5845, 1706-1709.

McNamara, J. P., Ziegler, A. D., Wood, S. H. & Vogler, J. B. 2006. Channel head locations with respect to geomorphologic thresholds derived from a digital elevation model: A case study in northern Thailand. *Forest Ecology and Management*, **224**, 1-2, 147-156.

Miller, D. J. 1961. *Geology of the Katalla district, Gulf of Alaska Tertiary province, Alaska*. U.S. Geological Survey Open-File Report.

Montgomery, D. R. & Foufoula-Georgiou, E. 1993. Channel network source representation using digital elevation models. *Water Resources Research*, **29**, 12, 3925-3934.

Moore, H. J. & Jakosky, B. M. 1989. Viking landing sites, remote-sensing observations, and physical properties of Martian surface materials. *Icarus*, **81**, 164-184.
Morton, D. M., Alvarez, R. M., Ruppert, K. R. & Goforth, B. 2008. Contrasting rainfall generated debris flows from adjacent watersheds at Forest Falls, southern California, USA. *Geomorphology*, **96**, 3-4, 322-338.
Moyle, W. R. 1982. *Water Resources of Borrego Valley and Vicinity, California: Phase 1 - Definition of Geologic and Hydrologic Characteristics of a Basin*. U.S. Geological Survey Open-File Report, **82-855**, USGS.
Musselwhite, D. S., Swindle, T. D. & Lunine, J. I. 2001. Liquid CO_2 breakout and the formation of recent small gullies on Mars. *Geophysical Research Letters*, **28**, 7, 1283-1285.
Mustard, J. F., Cooper, C. D. & Rifkin, M. K. 2001. Evidence for recent climate change on Mars from the identification of youthful near-surface ground ice. *Nature*, **412**, 6845, 411-414.
Norðdalh, H. 1990. Late Weichselian and early Holocene deglaciation history of Iceland. *Jökull*, **40**, 27-50.
Pelletier, J. D., Kolb, K. J., McEwen, A. S. & Kirk, R. L. 2008. Recent bright gully deposits on Mars: Wet or dry flow? *Geology*, **36**, 3, 211-214.
Perera, H. & Willgoose, G. 1998. A physical explanation of the cumulative area distribution curve. *Water Resources Research*, **34**, 5, 1335-1343.
Perron, J. T., Dietrich, W. E., Howard, A. D., McKean, J. A. & Pettinga, J. R. 2003. Ice-driven creep on Martian debris slopes. *Geophysical Research Letters*, **30**, 14, doi:10.1029/2003GL017603.
Perron, J. T., Kirchner, J. W. & Dietrich, W. E. 2009. Formation of evenly spaced ridges and valleys. *Nature*, **460**, 7254, 502-505.
Peters, G. H., Abbey, W., Bearman, G. H., Mungas, G. S., Smith, J. A., Anderson, R. C., Douglas, S. & Beegle, L. W. 2008. Mojave Mars simulant--Characterization of a new geologic Mars analog. *Icarus*, **197**, 2, 470-479.
Reiss, D., van Gasselt, S., Neukum, G. & Jaumann, R. 2004. Absolute dune ages and implications for the time of formation of gullies in Nirgal Vallis, Mars. *Journal of Geophysical Research - Planets*, **109**, E6, doi:10.1029/2004JE002251.
Schon, S. C., Head, J. W. & Fassett, C. I. 2009. Unique chronostratigraphic marker in depositional fan stratigraphy on Mars: Evidence for ca. 1.25 Ma gully activity and surficial meltwater origin. *Geology*, **37**, 3, 207-210.
Selby, M. J., 1993. *Hillslope Materials and Processes*. Oxford University Press, Oxford, 451 pp.
Shinbrot, T., Duong, N. H., Kwan, L. & Alvarez, M. M. 2004. Dry granular flows can generate surface features resembling those seen in Martian gullies. *Proceedings of the National Academy of Sciences of the United States of America*, **101**, 23, 8542-8546.
Sirkin, L. & Tuthill, S. J. 1987. Late Pleistocene and Holocene deglaciation and environments of the southern Chugach Mountains, Alaska. *Geological Society of America Bulletin*, **99**, 376-384.
Snyder, N. P., Whipple, K. X., Tucker, G. E. & Merritts, D. J. 2000. Landscape response to tectonic forcing: Digital elevation model analysis of stream profiles in the Mendocino triple junction region, Northern California. *Bulletin of the Geological Society of America*, **112**, 8, 1250-1263.
Soare, R. J. & Osinski, G. R. 2009. Stratigraphical evidence of late Amazonian periglaciation and glaciation in the Astapus Colles region of Mars. *Icarus*, **202**, 17-21.
Stock, J. & Dietrich, W. E. 2003. Valley incision by debris flows: Evidence of a topographic signature. *Water Resources Research*, **39**, 4, doi:10.1029/2001WR001057.

Stock, J. D. & Dietrich, W. E. 2006. Erosion of steepland valleys by debris flows. *Bulletin of the Geological Society of America*, **118**, 9-10, 1125-1148.

Tarboton, D. G., Bras, R. L. & Rodriguez-Iturbe, I. 1991. On the extraction of channel networks from digital elevation data. *Hydrological Processes*, **5**, 1, 81-100.

Tarboton, D. G. 1997. A new method for the determination of flow directions and upslope areas in grid digital elevation models. *Water Resources Research*, **33**, 2, 309-319.

Tarolli, P. & Fontana, G. D. 2009. Hillslope-to-valley transition morphology: New opportunities from high resolution DTMs. *Geomorphology*, **113**, 1-2, 47-56.

Treiman, A. H. 2003. Geologic settings of Martian gullies: Implications for their origins. *Journal of Geophysical Research - Planets;* , **108**, E4, doi:10.1029/2002JE001900.

Tucker, G. E. & Bras, R. L. 1998. Hillslope processes, drainage density, and landscape morphology. *Water Resources Research*, **34**, 10, 2751-2764.

van Gasselt, S., Hauber, E., Pio Rossi, A., Dumke, A., Orosei, R. & Neukum, G. 2010. Periglaical Geomorphology of Tempe Terra, Mars: role of mantling deposits in lobate debris apron formation and evolution. *In:* Balme, M., Bargery, A. S., Gallagher, C. & Gupta, S. (eds), *Geomorphology on Mars and Other Planets*. The Geological Society of London, in review.

Whipple, K. X. & Tucker, G. E. 1999. Dynamics of the stream-power river incision model: Implications for height limits of mountain ranges, landscape response timescales, and research needs. *Journal of Geophysical Research - Solid Earth*, **104**, B8, 17661-17674.

Williams, K. E., Toon, O. B., Heldmann, J. L. & Mellon, M. T. 2009. Ancient melting of mid-latitude snowpacks on Mars as a water source for gullies. *Icarus*, **200**, 2, 418-425.

Woods, R. A. & Sivapalan, M. 1997. A connection between topographically driven runoff generation and channel network structure. *Water Resources Research*, **33**, 12, 2939-2950.

Workman, J. B., Menges, C. M., Page, W. R., Taylor, E. M., Ekren, E. B., Rowley, P. D., Dixon, G. L., Thompson, R. A. & Wright, L. A. 2002. Geologic map of the Death Valley ground-water model area, Nevada and California, Miscellaneous Field Studies Map 2381-A. USGS.

Yetemen, O., Istanbulluoglu, E. & Vivoni, E. R. 2010. The implications of geology, soils, and vegetation on landscape morphology: Inferences from semi-arid basins with complex vegetation patterns in Central New Mexico, USA. *Geomorphology*, **116**, 3-4, 246-263.

Figure Captions

Fig. 1. HiRISE images of a variety of gullies on Mars. Image credits: NASA/JPL/UofA. (a) Gullies on the wall of a small impact crater within Kaiser Crater, site KC in this study, image number: PSP_003418_1335, at 18.8°E, 54.3°S. (b) Gullies within a polar pit, image number: PSP_003498_1090 at 1.6°E, 70.6°S. (c) Gullies on the wall of Galap Crater, near Sirenum Fossae, image number: PSP_003939_1420, at 192.9°E, 37.7°S. (d) Gullies on the wall of Wirtz Crater, a large impact crater to the east of Argyre basin, image number: PSP_002457_1310, at 335.3°E, 48.2°S. (e) Gullies on the slip face of dunes in Russell Crater, located in Noachis Terra, image number: PSP_001440_1255, at 12.9°E, 54.2°S. (f) Gullies on the wall of an impact crater to the west of Newton Crater in Terra Sirenum, image number: PSP_005930_1395, at 196.8°E, 40.3°S.

Fig. 2. Slope-area and Cumulative Area Distribution (CAD) plots, showing typical process domains on Earth. (a) Slope-area plot from Montgomery & Foufoula-Georgiou (1993) with the additional domain of Brardinoni & Hassan (2006) indicated with a dashed line. The arrows and dotted line indicate the adjustment to the alluvial domain boundary considering the gravitational acceleration of Mars. (b) CAD plot from McNamara *et al.* (2006). P(A>A*) represents the probability of a point in the landscape having a drainage area greater than the given drainage area, A*, on the x-axis. Region 1a represents hillslopes that diverge and do not gather drainage. Region 1b represents hillslopes with convergent topography. Region 1c represents pore-pressure triggered landsliding or debris flow. Region 2 represents incision, or channel formation. Region 3 has large steps where large tributaries join the channel.

Fig. 3. Hillshade representations made from digital elevation models of the study site locations on Earth. Areas included in this study are outlined and labelled in the Figure. (a) and (b) Site SJ, San Jacinto, California. (c) Site DV, Death Valley, California. (d) Site KA, St Elias Mountains, Alaska. (e) and (f) Site FR, Front Range, Colorado. (g) and (h) Site WF, Westfjords, NW Iceland.

Fig. 4. Hillshade representations made from digital elevation models of the study site locations on Mars. Areas included in this study are outlined and labelled in the Figure. (a) and (b) Site PC, Penticton Crater in Eastern Hellas. (c), (d) and (e) Site GC, Gasa Crater in Terra Cimmeria.(f) Site KC, a crater inside Kaiser Crater in Noachis Terra. (g) Site TS, a crater in Terra Sirenum. (h) The 10 km diameter synthetic crater, in which the square area is where the pink noise has been applied.

Fig. 5. Close-up views of gullies in Kaiser Crater (site KC), subset of HiRISE image PSP_003418_1335. Image credits: NASA/JPL/UofA. (a) Examples of gullyheads identified for individual slope-area analysis, marked by circles containing white crosses. (b) Levées interior to a channel, arrows point to levées within the channel on each side. (c) Single leveed channel, arrows point to the more obvious levee on the right, but there is an indication that there is another on the left as well.

Fig. 6. Slope-area plots for the study areas on Earth. Marked with solid grey lines are the domains of Montgomery & Foufoula-Georgiou (1993) and Brardinoni & Hassan (2006), as shown in Fig. 2a. Labels are included in (a), but omitted for clarity in the other plots and are as follows: (i) hillslopes domain, (ii) debris flow dominated channels, (iii) unchanneled valleys, (iv) alluvial channels and (v) debris flow deposition domain. The horizontal dotted

line represents the threshold for unconsolidated dry mass wasting at 0.7 gradient, which is equivalent to 35° slope.

(a) Plots for those areas dominated by talus and creep processes. (b) Plots for those areas dominated by debris flow, with some influence from talus processes. (c) Plots for those areas dominated by debris flow, with influence from alluvial processes. (d) Plots for those areas dominated by ephemeral water flow, or alluvial processes.

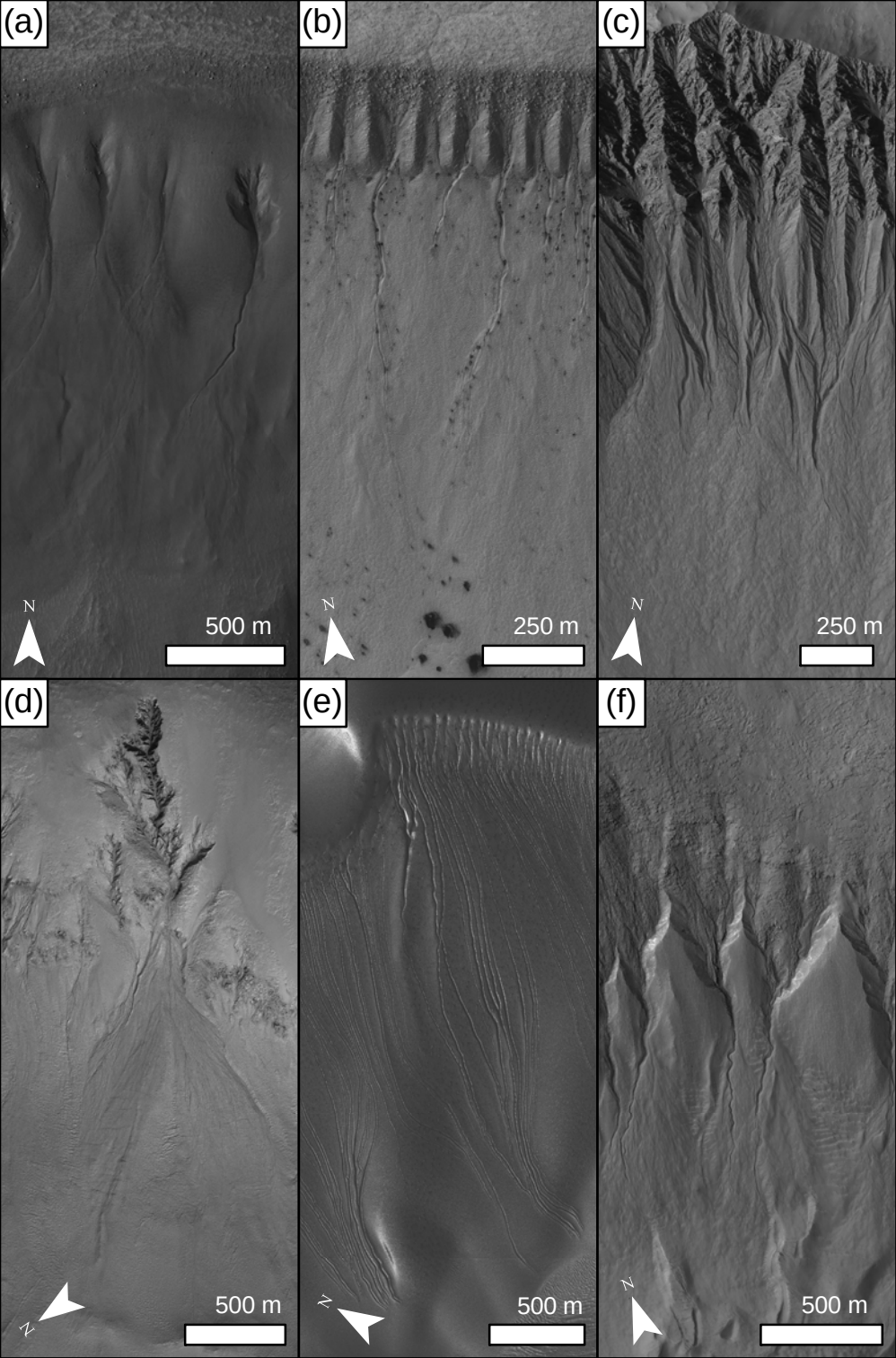
Fig. 7. Cumulative Area Distribution plots for the study areas on Earth. (a) Plots for those areas dominated by talus and creep processes. (b) Plots for those areas dominated by debris flow, with some influence from talus processes. (c) Plots for those areas dominated by debris flow, with influence from alluvial processes. (d) Plots for those areas dominated by ephemeral water flow, or alluvial processes.

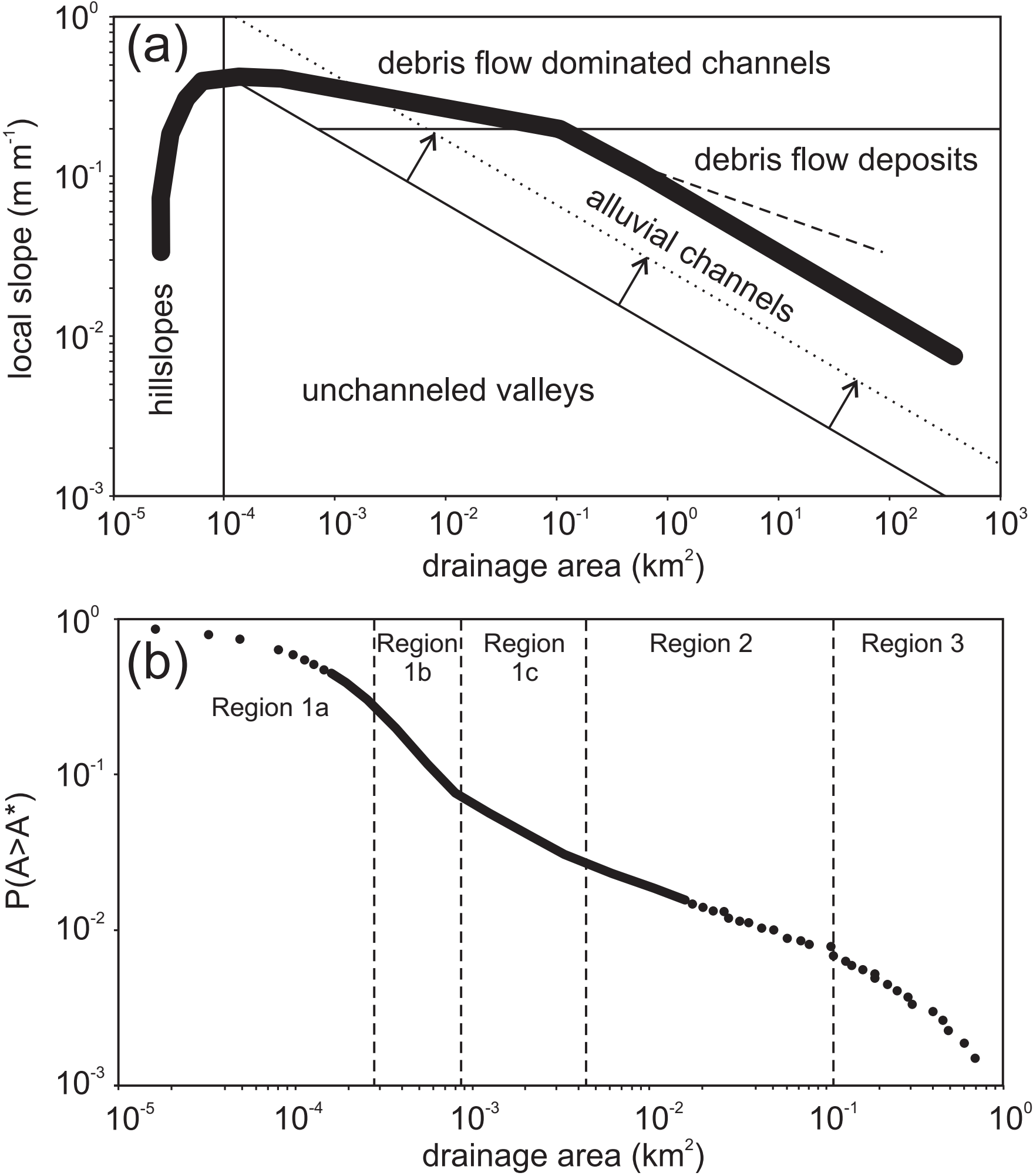
Fig. 8. Slope-area plots for the study areas on Mars. Marked with solid grey lines are the domains of Montgomery & Foufoula-Georgiou (1993) and Brardinoni & Hassan (2006), as shown in Fig. 2a. Labels are included in (a), but omitted for clarity in the other plots and are as follows: (i) hillslopes domain, (ii) debris flow dominated channels, (iii) unchanneled valleys, (iv) alluvial channels and (v) debris flow deposition domain. The horizontal dotted line represents the threshold for unconsolidated dry mass wasting at 0.7 gradient, which is equivalent to 35° slope. The dash-dot line represents the adjustment of the alluvial domain when taking into account Mars' gravitational acceleration. (a) Plots for Site PC, Penticton Crater in Eastern Hellas. (b) Plots for Site GC, Gasa Crater in Terra Cimmeria. (b) Plots for Site KC, a crater inside Kaiser Crater in Noachis Terra. (d) Plots for Site TS, a crater in Terra Sirenum and the 10 km diameter synthetic crater.

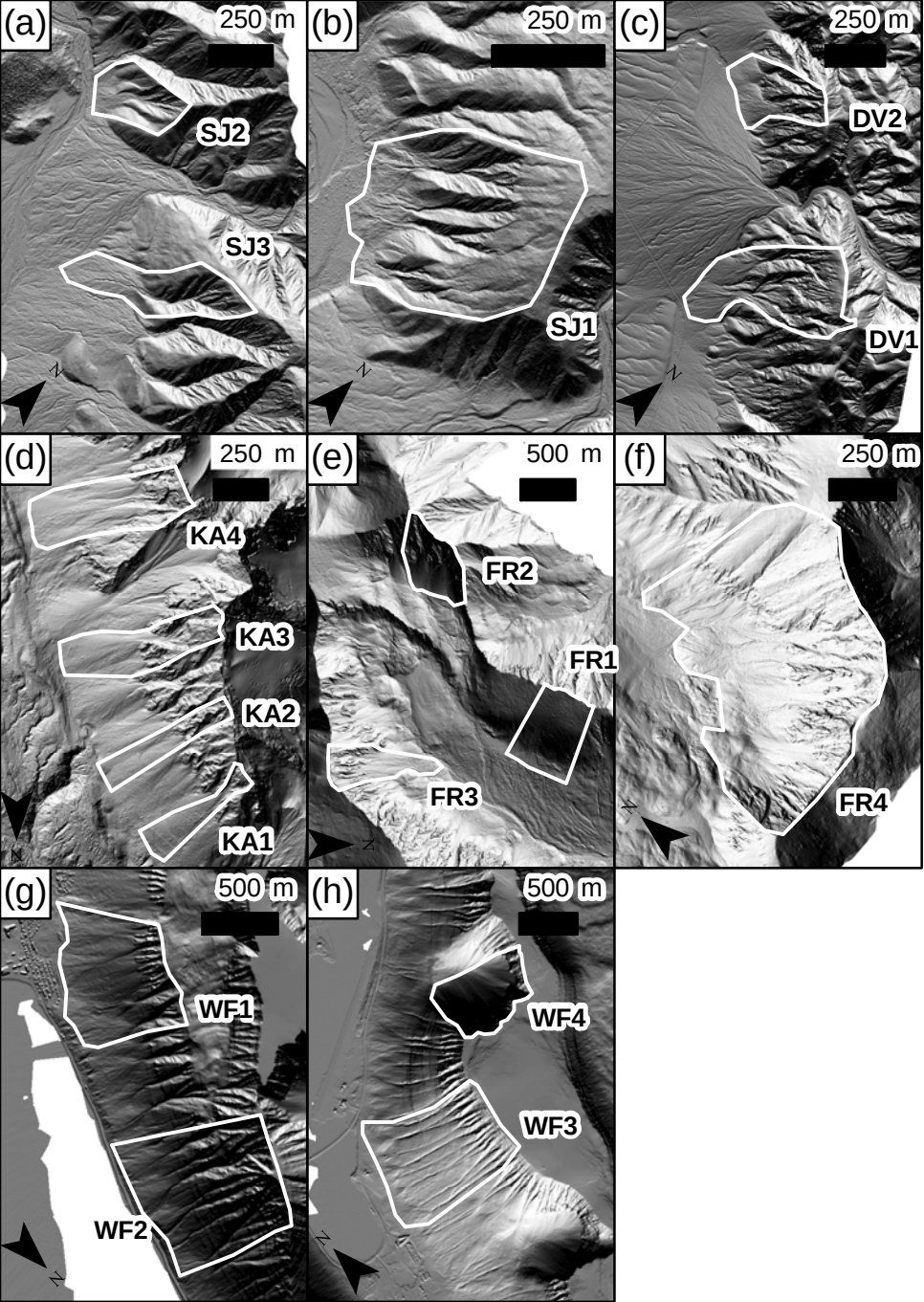
Fig. 9. Cumulative Area Distribution plots for the study areas on Mars. (a) Plots for Site PC, Penticton Crater in Eastern Hellas. (b) Plots for Site GC, Gasa Crater in Terra Cimmeria. (b) Plots for Site KC, a crater inside Kaiser Crater in Noachis Terra. (d) Plots for Site TS, a crater in Terra Sirenum and the 10 km diameter synthetic crater.

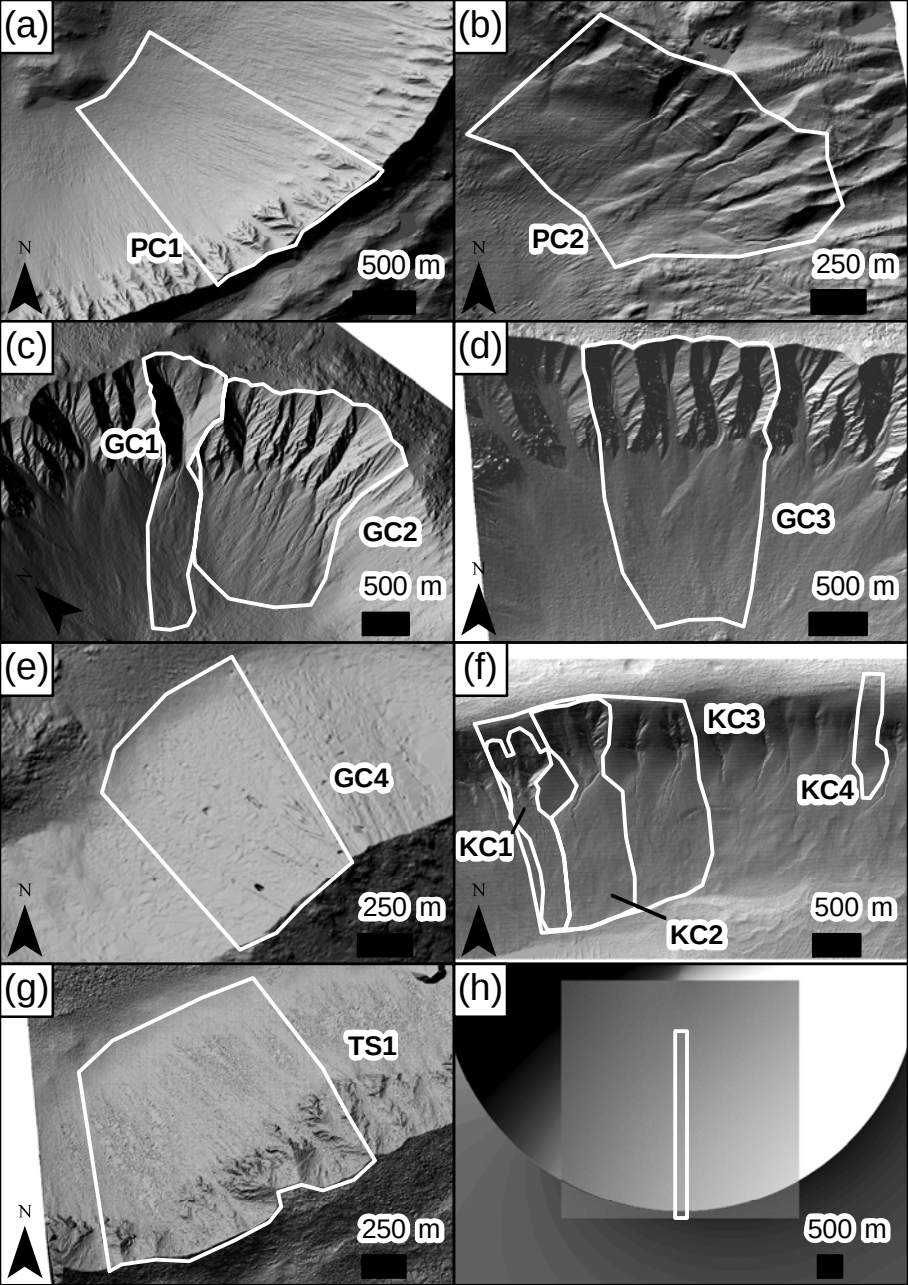
Fig. 10. Wetness index maps made from digital elevation models of the study site locations on Earth. Areas included in this study are outlined and labelled in the Figure. Wetness index values are represented by the same colours in Fig. 11 to allow direct comparison. (a) and (b) Site SJ, San Jacinto, California. (c) Site DV, Death Valley, California. (d) Site KA, St Elias Mountains, Alaska. (e) and (f) Site FR, Front Range, Colorado. (g) and (h) Site WF, Westfjords, NW Iceland.

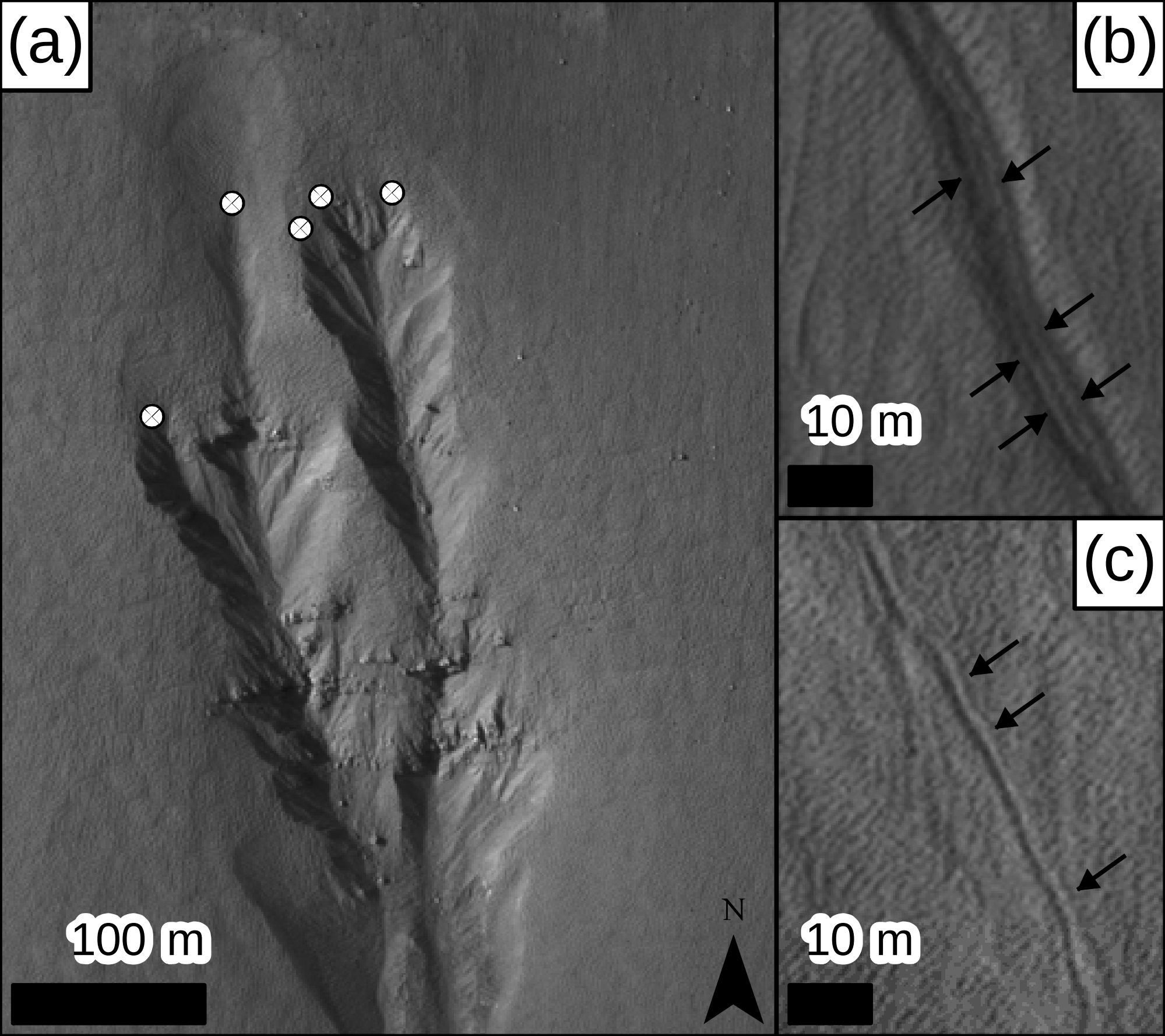
Fig. 11. Wetness index maps made from digital elevation models of the study site locations on Mars. Areas included in this study are outlined and labelled in the Figure. Wetness index values are represented by the same colours in Fig. 10 to allow direct comparison. (a) and (b) Site PC, Penticton Crater in Eastern Hellas. (c), (d) and (e) Site GC, Gasa Crater in Terra Cimmeria.(f) Site KC, a crater inside Kaiser Crater in Noachis Terra. (g) Site TS, a crater in Terra Sirenum. (h) 10 km diameter synthetic crater.

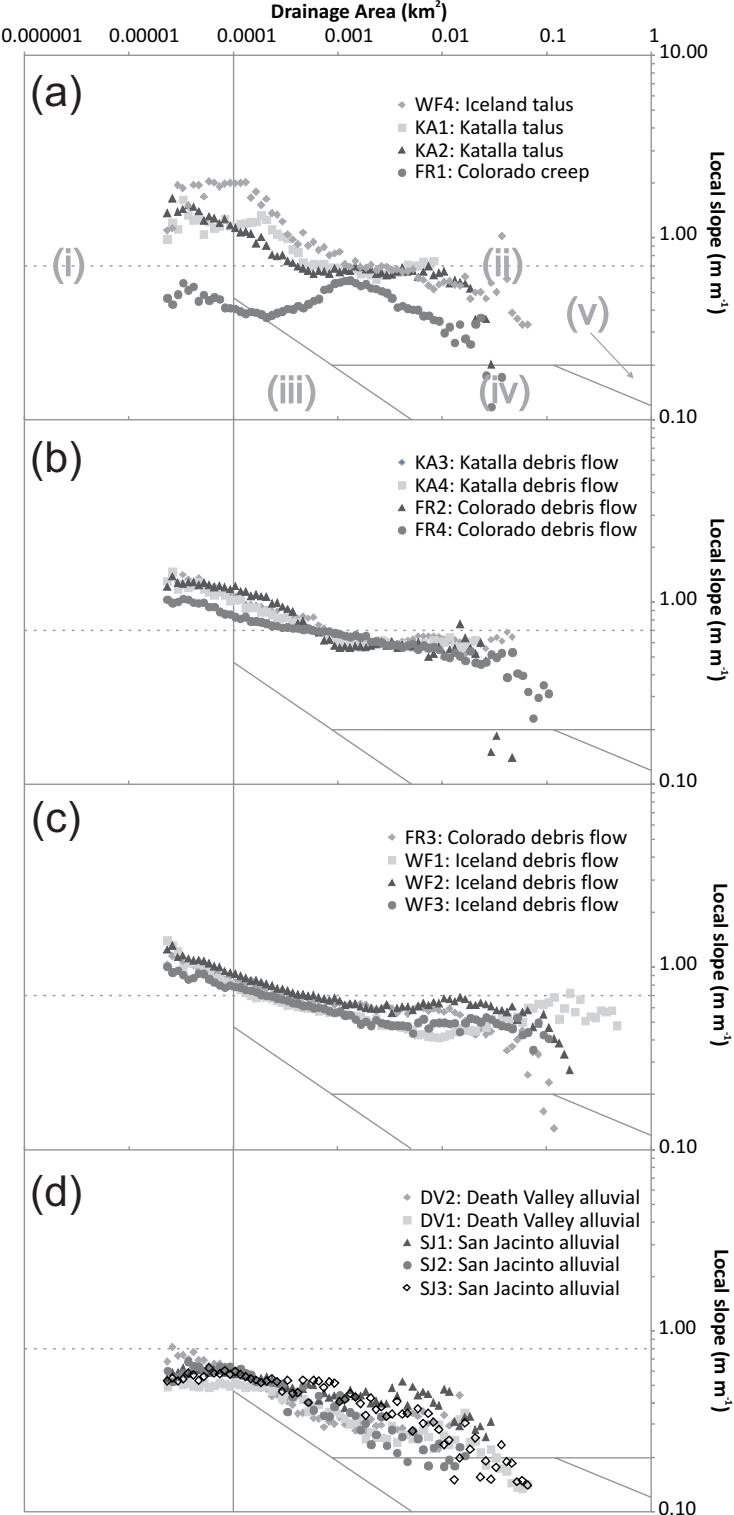

(a)
N
500 m
(b)
N
250 m
(c)
N
250 m
(d)
N
500 m
(e)
N
500 m
(f)
N
500 m

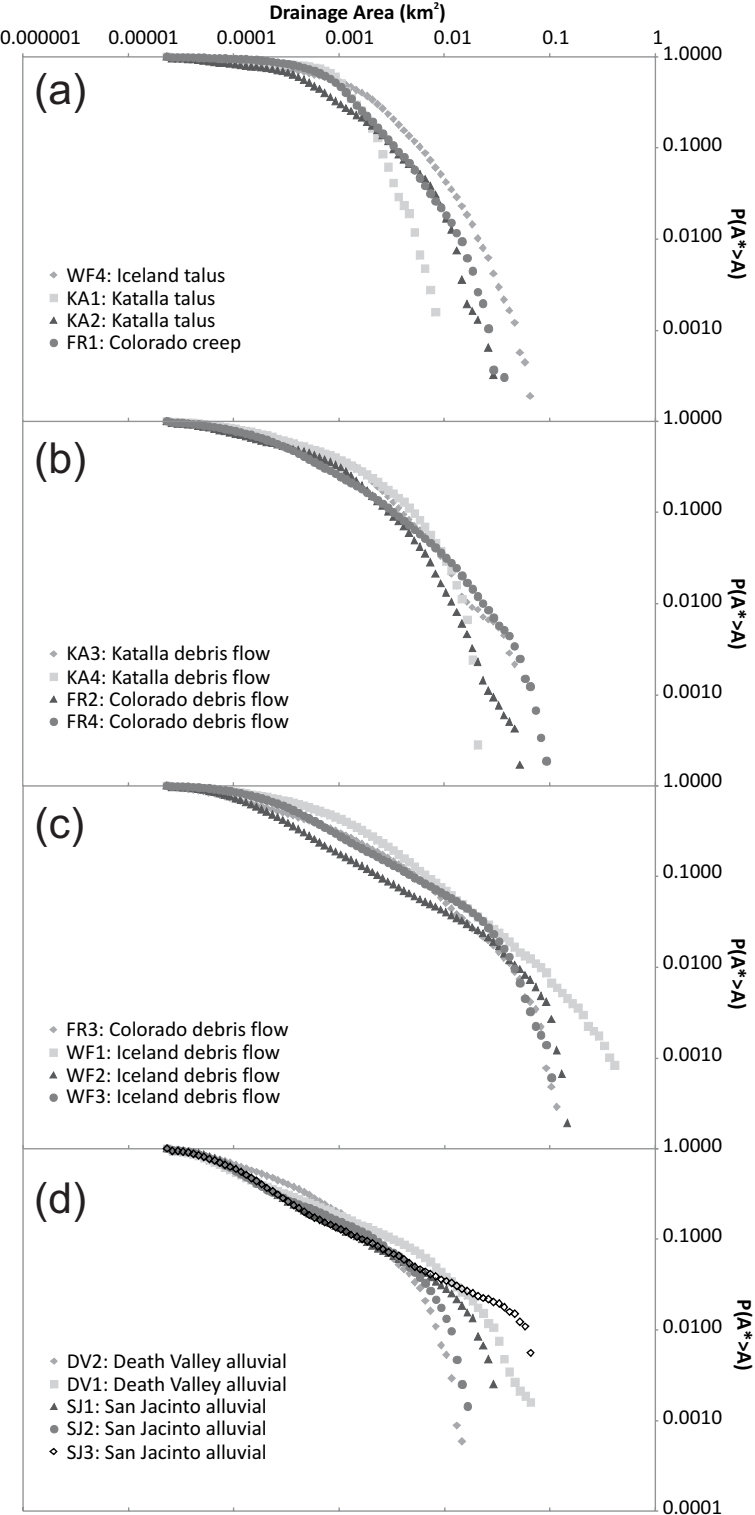

(a)
debris flow dominated channels
debris flow deposits
alluvial channels
unchanneled valleys
hillslopes
local slope (m m-1)
drainage area (km2)
(b)
Region 1a
Region 1b
Region 1c
Region 2
Region 3
P(A>A*)
drainage area (km2)

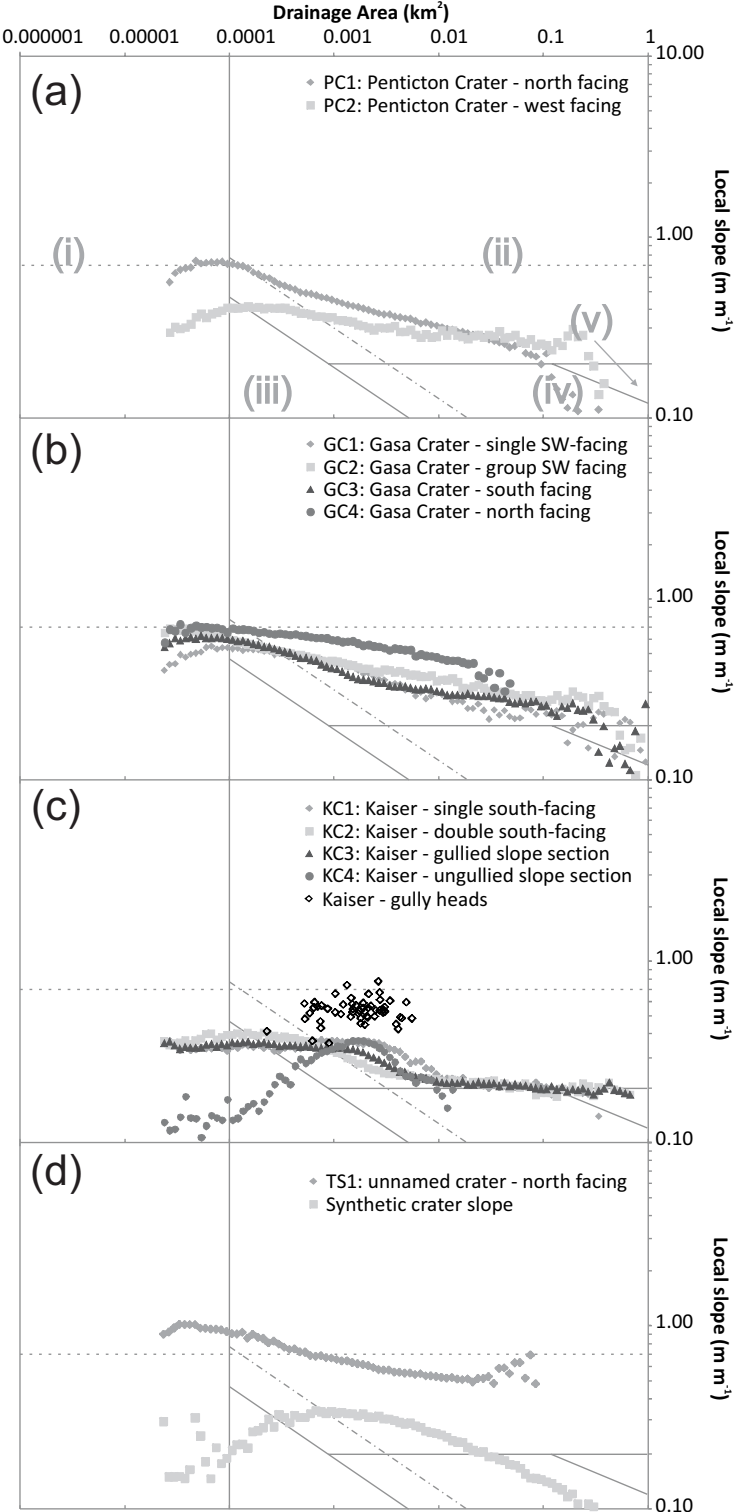

(a)
250 m
SJ2
SJ3
(b)
250 m
SJ1
(c)
250 m
DV2
DV1
(d)
250 m
KA4
KA3
KA2
KA1
(e)
500 m
FR2
FR1
FR3
(f)
250 m
FR4
(g)
500 m
WF1
WF2
(h)
500 m
WF4
WF3

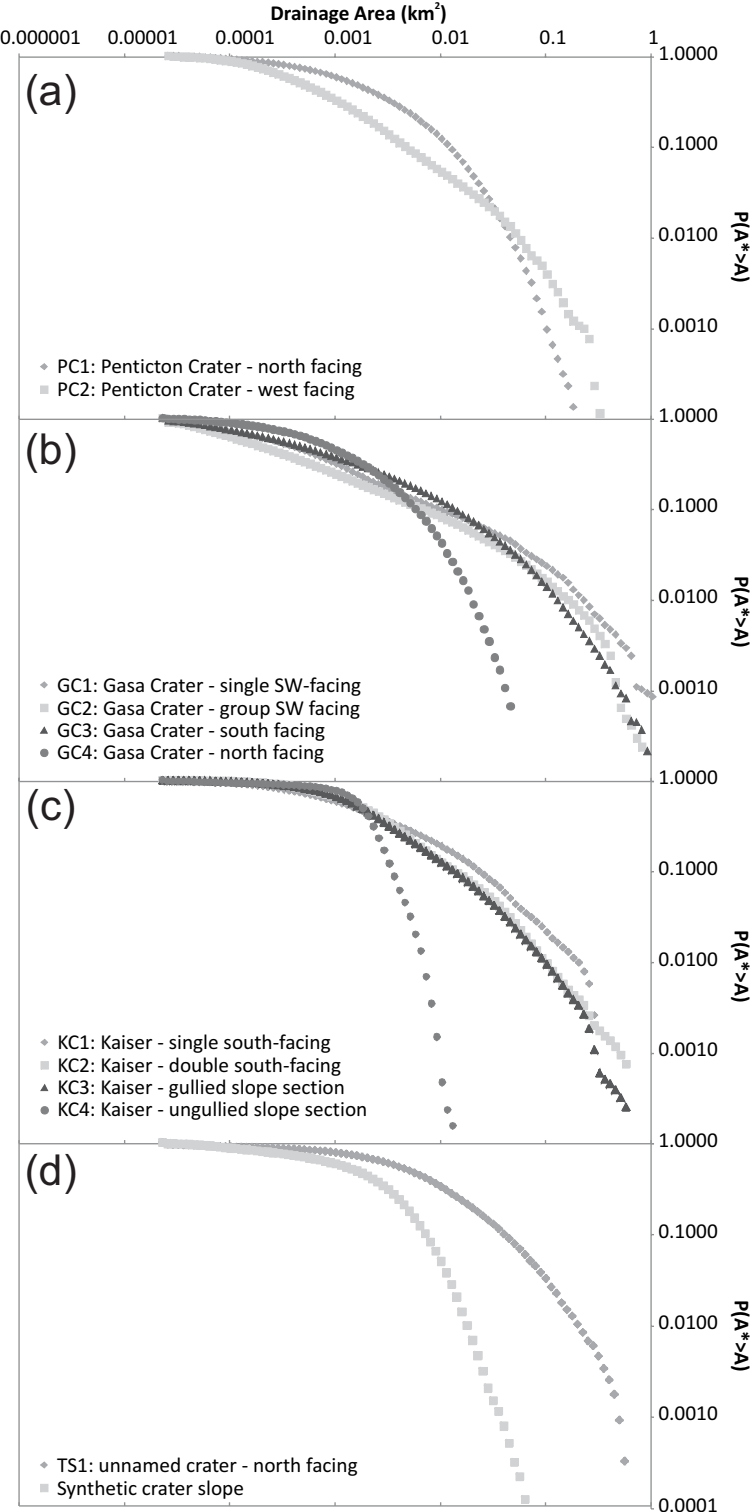

(a)
PC1
N
500 m
(b)
PC2
N
250 m
(c)
GC1
GC2
N
500 m
(d)
GC3
N
500 m
(e)
GC4
N
250 m
(f)
KC3
KC4
KC1
KC2
N
500 m
(g)
TS1
N
250 m
(h)
500 m

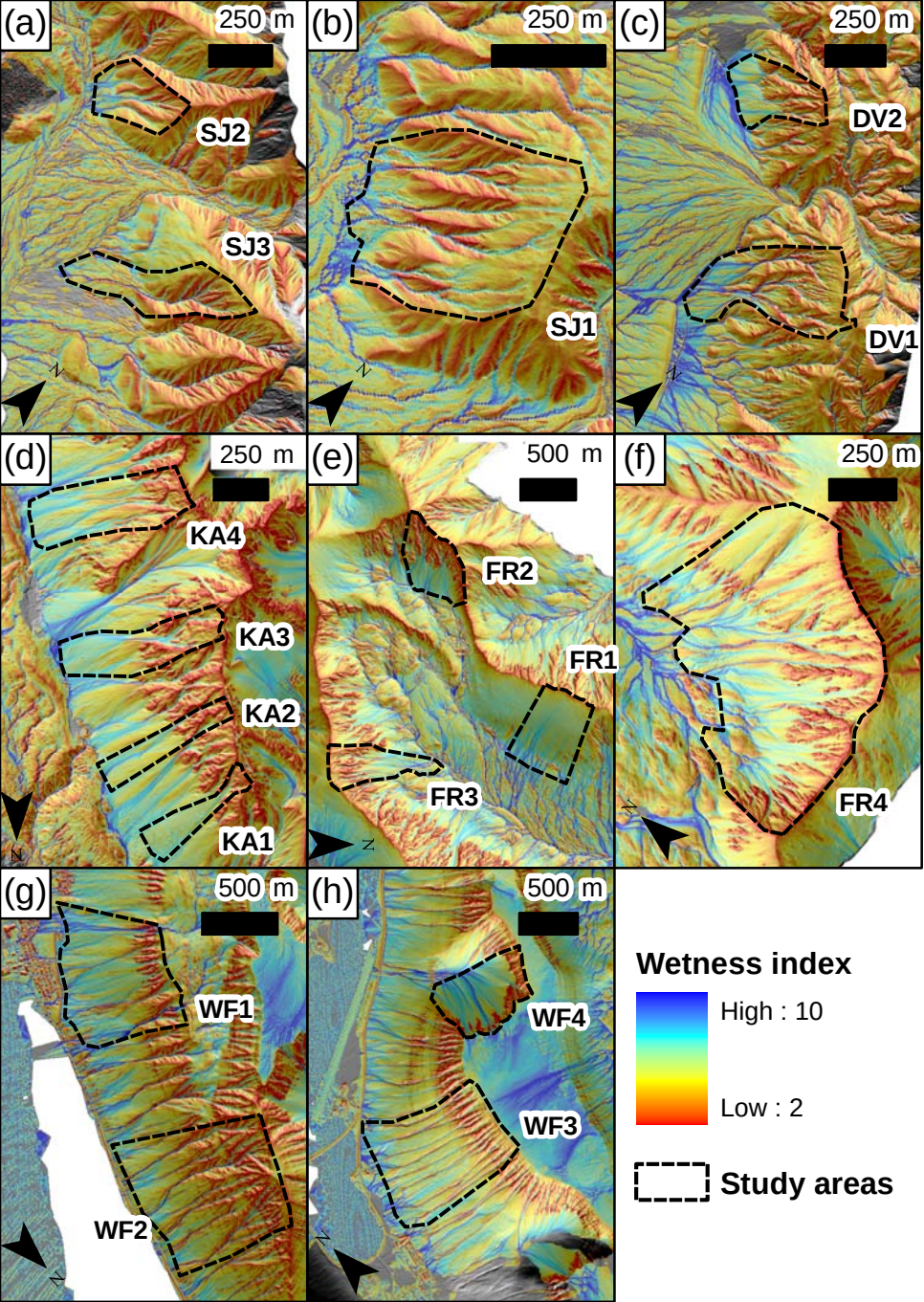

(a)
100 m
N
(b)
10 m
(c)
10 m


Drainage Area (km²)
0.000001
0.00001
0.0001
0.001
0.01
0.1
1
10.00
1.00
0.10
Local slope (m m⁻¹)
(a)
WF4: Iceland talus
KA1: Katalla talus
KA2: Katalla talus
FR1: Colorado creep
(i)
(ii)
(iii)
(iv)
(v)
(b)
KA3: Katalla debris flow
KA4: Katalla debris flow
FR2: Colorado debris flow
FR4: Colorado debris flow
(c)
FR3: Colorado debris flow
WF1: Iceland debris flow
WF2: Iceland debris flow
WF3: Iceland debris flow
(d)
DV2: Death Valley alluvial
DV1: Death Valley alluvial
SJ1: San Jacinto alluvial
SJ2: San Jacinto alluvial
SJ3: San Jacinto alluvial


Drainage Area (km²)
0.000001
0.00001
0.0001
0.001
0.01
0.1
1
(a)
WF4: Iceland talus
KA1: Katalla talus
KA2: Katalla talus
FR1: Colorado creep
(b)
KA3: Katalla debris flow
KA4: Katalla debris flow
FR2: Colorado debris flow
FR4: Colorado debris flow
(c)
FR3: Colorado debris flow
WF1: Iceland debris flow
WF2: Iceland debris flow
WF3: Iceland debris flow
(d)
DV2: Death Valley alluvial
DV1: Death Valley alluvial
SJ1: San Jacinto alluvial
SJ2: San Jacinto alluvial
SJ3: San Jacinto alluvial
P(A*>A)
1.0000
0.1000
0.0100
0.0010
0.0001


Drainage Area (km²)
0.000001
0.00001
0.0001
0.001
0.01
0.1
1
(a)
PC1: Penticton Crater - north facing
PC2: Penticton Crater - west facing
(i)
(ii)
(iii)
(iv)
(v)
(b)
GC1: Gasa Crater - single SW-facing
GC2: Gasa Crater - group SW facing
GC3: Gasa Crater - south facing
GC4: Gasa Crater - north facing
(c)
KC1: Kaiser - single south-facing
KC2: Kaiser - double south-facing
KC3: Kaiser - gullied slope section
KC4: Kaiser - ungullied slope section
Kaiser - gully heads
(d)
TS1: unnamed crater - north facing
Synthetic crater slope
Local slope (m m⁻¹)
10.00
1.00
0.10


Drainage Area (km²)
0.000001
0.00001
0.0001
0.001
0.01
0.1
1
(a)
PC1: Penticton Crater - north facing
PC2: Penticton Crater - west facing
(b)
GC1: Gasa Crater - single SW-facing
GC2: Gasa Crater - group SW facing
GC3: Gasa Crater - south facing
GC4: Gasa Crater - north facing
(c)
KC1: Kaiser - single south-facing
KC2: Kaiser - double south-facing
KC3: Kaiser - gullied slope section
KC4: Kaiser - ungullied slope section
(d)
TS1: unnamed crater - north facing
Synthetic crater slope
P(A*>A)
1.0000
0.1000
0.0100
0.0010
0.0001


(a)
250 m
SJ2
SJ3
(b)
250 m
SJ1
(c)
250 m
DV2
DV1
(d)
250 m
KA4
KA3
KA2
KA1
(e)
500 m
FR2
FR1
FR3
(f)
250 m
FR4
(g)
500 m
WF1
WF2
(h)
500 m
WF4
WF3
Wetness index
High : 10
Low : 2
Study areas

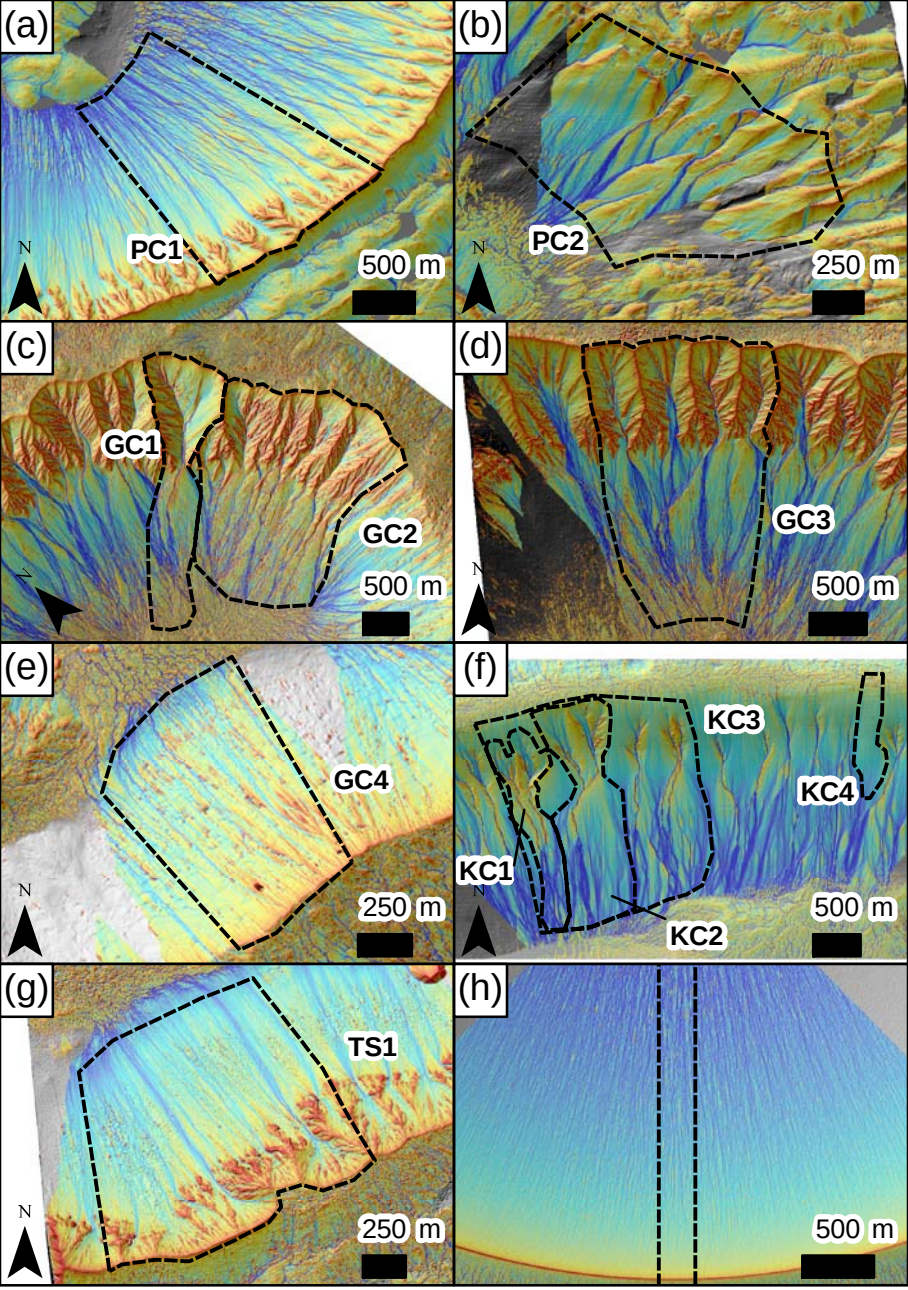

(a)
PC1
N
500 m
(b)
PC2
N
250 m
(c)
GC1
GC2
N
500 m
(d)
GC3
N
500 m
(e)
GC4
N
250 m
(f)
KC3
KC4
KC1
KC2
N
500 m
(g)
TS1
N
250 m
(h)
500 m
Wetness Index:
10
2

Table 1. *Summary table for the study sites on Earth*

Site	Location	Date Flown	Data Source	Approx. precipitation (mm/year)	Landscape-type	Latitude	Longitude	Average elevation (m)	Relief (m)
A	San Jacinto Fault (SJF Segment 3) - Santa Rosa Mountains	mid 2005	NCALM B4 Project	150	desert	33° 25' 58.55" N	116° 28' 57.55" W	597	677
B	Death Valley California	28/02/2005	NCALM	<85	desert	39° 38' 01.77" N	105° 49' 13.88" W	3664	1345
C	St. Elias, Alaska	02-15/9/2005	NCALM	2000	periglacial	60° 18' 18.59" N	144° 32' 14.98" W	490	831
D	Front Range, Colorado	30/09/2005	NCALM	600	periglacial	37° 04' 28.50" N	117° 26' 37.60" W	258	854
E	Westfjords, Iceland	05/08/2007	ARSF	700	periglacial	66° 04' 13.20" N	023° 07' 14.19" W	271	807

Average elevation is given relative to datum, for A-D this is NAD 1983 and for Site E this is WGS 1984, in both cases the difference between the datum and sea level is approximately 60 m. Abbreviations: NCALM - National Center for Airborne Laser Mapping supported by the USA's National Science Foundation, ARSF – Airborne Research and Survey Facility supported by the UK Natural Environment Research Council.

Table 2. *Summary table for the study sites on Mars*

Site	HiRISE image pair	Latitide	Longitude	Average elevation (m)	Relief (m)
F	PSP_001714_1415 PSP_001846_1415	-38.4°	96.8°	-2648	1124
G	PSP_004060_1440 PSP_005550_1440	-35.7°	129.4°	300	1205
H	PSP_003418_1335 PSP_003708_1335	-46.1°	18.8°	595	687
J	PSP_003674_1425 PSP_005942_1425	-37.4°	229.0°	1904	961

.

Average elevation is given relative to the Mars datum, as defined from the MOLA dataset. The average elevation has been estimated from the MOLA dataset and relief from the HiRISE DEMs.